

1 **LAMINAR MECHANISMS OF SACCADIC SUPPRESSION IN PRIMATE VISUAL**
2 **CORTEX**

3 Sachira Denagamage^{1,2}, Mitchell P. Morton^{1,2}, John H. Reynolds⁴, Monika P. Jadi^{1,2,3,*} and
4 Anirvan S. Nandy^{1,2,*}

5 ¹Department of Neuroscience, Yale University, New Haven, CT 06511

6 ²Interdepartmental Neuroscience Program, Yale University, New Haven, CT 06511

7 ³Department of Psychiatry, Yale University, New Haven, CT 06511

8 ⁴Systems Neurobiology Laboratories, The Salk Institute for Biological Studies, La Jolla, CA 92037

9 *co-senior and corresponding authors

10 Correspondence: monika.jadi@yale.edu, anirvan.nandy@yale.edu

11

12 **ABSTRACT**

13 Saccades are a ubiquitous and crucial component of our visual system, allowing for the efficient
14 deployment of the fovea and its accompanying neural resources. Initiation of a saccade is known
15 to cause saccadic suppression, a temporary reduction in visual sensitivity^{1,2} and visual cortical
16 firing rates³⁻⁶. While saccadic suppression has been well characterized at the level of perception
17 and single neurons, relatively little is known about the visual cortical networks governing this
18 phenomenon. Here we examine the effects of saccadic suppression on distinct neural
19 subpopulations within area V4. We find cortical layer- and cell type-specific differences in the
20 magnitude and timing of peri-saccadic modulation. Neurons in the input layer show changes in
21 firing rate and inter-neuronal correlations prior to saccade onset, suggesting that this layer receives
22 information about impending saccades. Putative inhibitory interneurons in the input layer elevate
23 their firing rate during saccades and may suppress the activity of other cortical subpopulations. A

24 computational model of this circuit recapitulates our empirical observations and demonstrates that
25 an input layer-targeting pathway can initiate saccadic suppression by enhancing local inhibitory
26 activity. Together, our results provide a mechanistic understanding of how eye movement
27 signaling interacts with cortical circuitry to enforce visual stability.

28

29 **INTRODUCTION**

30 As we observe the world around us, our eyes dart from point to point. Each of these shifts in gaze
31 is a saccade – a ballistic movement of both eyes. Saccades significantly improve the efficiency of
32 the primate visual system by allowing us to flexibly deploy our fovea, the dedicated high acuity
33 zone at the center of the retina, towards objects of interest in our environment. However, saccades
34 also pose a substantial challenge for ongoing visual processing, as each saccade produces abrupt
35 and rapid motion across the retina. Therefore, saccades are also accompanied by a temporary
36 reduction in visual sensitivity, termed saccadic suppression, that serves to blunt our perception of
37 this motion^{1,2}. Perhaps reflecting the diminished sensory processing during saccades, the firing
38 rates of neurons in many regions of the visual cortex are also transiently suppressed³⁻⁶. Yet, despite
39 extensive psychophysical characterization and single neuron electrophysiological analysis,
40 relatively little is known about the circuit level mechanisms underlying saccadic suppression in
41 the visual cortex. One prevailing hypothesis suggests that saccadic suppression is mediated by a
42 corollary discharge signal originating in the brain regions responsible for initiating eye
43 movements⁷⁻⁹. Given the synaptic and motor delays accompanying the execution of the saccadic
44 motor command, a coincident corollary discharge to the visual cortex could trigger compensatory
45 mechanisms prior to the start of the eye movement. Consistent with this idea, changes in neural
46 activity before saccade onset have been observed in several visual cortical areas⁵. However, in

47 spite of clear neural evidence that the visual cortex receives information about upcoming saccades,
48 the pathway by which a saccadic signal arrives in the visual cortex is unknown, and how that signal
49 interacts with local circuitry to mediate saccadic suppression remains unclear.

50 We examined these questions within area V4, a critical hub in the visual processing stream
51 responsible for object recognition¹⁰. V4 is known to exhibit saccadic suppression in both humans⁴
52 and macaques⁶, and undergoes dynamic shifts in stimulus sensitivity during the preparation of
53 saccades¹¹. To investigate the underlying neural mechanisms, we studied saccadic suppression in
54 the context of the laminar cortical circuit, which is composed of six layers with highly stereotyped
55 patterns of intra- and inter-laminar connectivity^{12,13}. In higher-order visual areas, such as V4, layer
56 IV (the *input* layer) is the primary target of projections carrying visual information from lower-
57 order areas, such as V1, V2, and V3^{14,15}. After arriving in the input layer, visual information is
58 then processed by local neural subpopulations as it is sent to layers II/III (the *superficial* layer) and
59 layers V/VI (the *deep* layer), which serve as output nodes in the laminar circuit^{12,16}. In V4, the
60 superficial and deep layers feed information forward to downstream visual areas, such as ST¹⁷,
61 TEO¹⁸, and TE¹⁹. Alongside feedforward input from lower-order visual areas, V4 also receives
62 projections from other cortical regions, such as the prefrontal cortex¹⁵, as well as from subcortical
63 structures²⁰. Accordingly, several pathways targeting V4 could be responsible for relaying
64 information about upcoming saccades: 1) projections from lower visual areas (V1/V2/V3), which
65 predominantly target the input layer^{14,15}, 2) a projection from the frontal eye fields (FEF), which
66 predominantly targets the superficial and deep layers^{21,22}, and 3) a projection from the pulvinar,
67 which predominantly targets the superficial and input layers²³⁻²⁵. Neurons in V1^{26,27}, FEF²⁸⁻³⁰, and
68 pulvinar³¹⁻³³ are known to respond to saccades, and the corresponding pathways are therefore
69 strong candidates for initiating saccadic suppression in V4.

70 Given the organization of cortical circuitry, we reasoned that a saccadic signaling pathway
71 should target the site of entry for visual information, the input layer, to most efficiently suppress
72 visual processing. Furthermore, in light of the similarities between peri-saccadic stimulus
73 processing and general reductions in visual gain^{6,26}, we considered whether saccadic suppression
74 might be mediated in a manner comparable to visual gain modulation. Specifically, we
75 hypothesized that an elevation in local inhibitory activity, a common mechanism for gain control³⁴⁻
76 ³⁶, functionally suppresses neural processing in V4 during saccades. We sought to confirm our
77 predictions by utilizing a cortical layer-specific recording approach in combination with
78 electrophysiological cell type classification to simultaneously record from six well-defined neural
79 subpopulations in V4.

80

81 **RESULTS**

82 **Dissociating the Effects of Vision and Eye Movements**

83 Past approaches for studying saccadic modulation have typically involved cued saccade
84 tasks^{4,6,26,37}, which risk conflating the neural effects of visual stimulus processing with the neural
85 effects of saccades. To dissociate saccadic signaling from visually induced activity in area V4, we
86 performed a series of spontaneous recordings while two rhesus macaques were seated in the dark.
87 We found that despite their inability to observe specific objects in the environment, both animals
88 continued to make saccades freely under these conditions. We identified individual saccades by
89 estimating the onset and offset times of ballistic eye movements (see Methods). In order to remove
90 fixational eye movements (microsaccades), we discarded saccades with amplitudes less than 0.7
91 degrees of visual angle. Additionally, to prevent the effects of one eye movement from overlapping
92 with those of the next, we only included saccades that were separated from one another by at least

93 500 ms. This approach provided us with a set of 4420 saccades that were used for all subsequent
94 analyses. We evaluated the quality of our eye movement dataset by examining amplitude and
95 velocity traces from individual saccades, as well as by characterizing the main sequence. The main
96 sequence is the approximately linear amplitude-velocity relationship observed across all
97 saccades³⁸, which we found held true for our data (Figure 1A).

98 While the monkeys were making spontaneous saccades, we simultaneously recorded
99 neural activity from well-isolated single-units ($n = 211$), multi-units ($n = 110$), and local field
100 potentials (LFPs) using linear array probes in area V4. The use of recording chambers containing
101 an optically-transparent artificial dura allowed us to make electrode penetrations perpendicular to
102 the cortical surface, and therefore in good alignment with individual cortical columns (see
103 Methods). The alignment of each penetration was confirmed by mapping receptive fields along
104 the depth of cortex, with overlapping receptive fields indicating proper alignment (Figure 1B).
105 Laminar boundaries were identified with current source density (CSD) analysis^{39,40}. The CSD,
106 defined as the second spatial derivative of the LFP, maps the location of current sources and sinks
107 along the depth of the probe. Each layer of the visual cortex produces a characteristic current
108 source-sink pattern in response to visual stimulation, with the input layer producing a current sink
109 followed by a current source, and the superficial and deep layers producing the opposite pattern of
110 activity (Figure 1C). By identifying transitions between current sources and sinks, we assigned
111 laminar identities to each of our recording sites (Figure 1D – LFP traces colored by layer). We
112 also separated well-isolated single-units into two populations on the basis of their waveform
113 duration: narrow-spiking units, corresponding to putative inhibitory interneurons, and broad-
114 spiking units, corresponding to putative excitatory neurons (Figure 1D – spikes colored by unit

115 type)⁴¹⁻⁴³. The three cortical layers and two unit types thus gave us six distinct neural
116 subpopulations to consider in subsequent analyses.

117

118 **Narrow-Spiking Input Layer Units Show Positive Peri-Saccadic Modulation**

119 To evaluate neural subpopulation-specific responses, we first estimated the peri-saccadic firing
120 rate of well-isolated single-units with a kernel-based approach, in which each spike is convolved
121 with a gaussian kernel⁴⁴ (Figure S1). We selected the kernel bandwidth on a unit-by-unit basis at
122 each point in time using an optimization algorithm that minimizes mean integrated squared error⁴⁵.
123 When looking at units grouped by cell type, narrow-spiking units exhibit less peri-saccadic
124 suppression than broad-spiking units (Figure 2A). The cause of this difference became clear when
125 the units were further separated by layer. All laminar subpopulations of broad-spiking units
126 displayed peri-saccadic suppression, as did narrow-spiking units in the superficial and deep layers.
127 In contrast, narrow-spiking input layer units elevated their firing rate in response to a saccade
128 (Figure 2B-C; see Figure S2 for additional single-unit examples).

129 To quantify these observations, we calculated a modulation index that represents the degree
130 to which the firing rate of each unit deviated from its pre-saccadic baseline activity (see Methods).
131 We found that narrow-spiking input layer units were the only group with a positive modulation
132 index, which was significantly different from most other subpopulations (Figure 2D). We also
133 noted that at the single-unit level, each of the six subpopulations had some proportion of positively
134 modulated units (Figure S3). Therefore, the difference in subpopulation level firing rates could be
135 caused by narrow-spiking input layer neurons having a greater average magnitude of positive
136 modulation, or by having a greater proportion of positively modulated units. We determined both
137 to be true. Narrow-spiking input layer neurons displayed a larger magnitude of positive modulation

138 (Figure 2E), and were also more likely to be positively modulated (Figure 2F). We found it
139 particularly striking that, in accordance with our hypothesis, only narrow-spiking input layer units
140 (i.e. putative inhibitory interneurons) showed an enhancement in firing. This led us to believe that
141 an elevation in input layer inhibitory activity could be responsible for the peri-saccadic suppression
142 of firing within the visual cortex reported previously³⁻⁶.

143

144 **Input Layer Units Respond Prior to Saccades**

145 In order to gate out visual signals received during a saccade, neurons in the cortical layer initiating
146 suppression would need to be activated prior to the start of the eye movement. To confirm that this
147 was true for the input layer, we performed a timing analysis to determine whether any of the
148 recorded subpopulations show significant changes in firing rate prior to saccade onset. For each
149 single-unit, we found the time at which their activity first deviated outside a 95% confidence
150 interval calculated from their pre-saccadic baseline activity, an event that was marked as the time
151 of first significant response. The results of this approach for six example units (the same example
152 units as in Figure S1) are illustrated in Figure 3A. While there was response variability at the level
153 of single-units, the input layer subpopulations (both narrow- and broad-spiking) were the only ones
154 that responded prior to saccade onset (Figure 3B). This provides strong evidence that the input
155 layer receives information about upcoming saccades with sufficient time to enact changes in
156 activity throughout the cortical column.

157

158 **Saccades Increase Correlated Variability in the Input Layer**

159 If input layer neurons receive pre-saccadic excitation from a common source, that signaling should
160 also manifest itself as an increase in correlated variability among pairs of input layer units prior to

161 saccade onset. To test this, we computed spike count correlations (SCC) between pairs of
162 simultaneously recorded single- and multi-units as a function of time, and pooled these results into
163 six groups on the basis of their pairwise laminar locations. All pair types showed a substantial
164 increase in SCC around the time of saccades (Figure S4A). We quantified the precise time at which
165 correlations first began to rise with a bootstrapping analysis (see Methods). SCC began increasing
166 prior to saccade onset in input-input pairs (Figure 4A), but after saccade onset in all other pairs
167 (Figure 4B). This pattern of activity is consistent with the pre-saccadic arrival of a signal that is
168 shared among input layer units. The delayed response of all other pair types suggests that they
169 inherit their activity from the input layer. Additionally, the precise time at which input-input
170 correlations began to rise (~40 ms before saccade onset) is remarkably similar to the time at which
171 input layer units began to show firing rate modulation (also ~40 ms before saccade onset), further
172 indicating that these two observations have a common cause: the activation of a saccadic signaling
173 pathway.

174 Alongside the expected rise in correlations, we also found a reduction in correlations that
175 began ~250 ms prior to saccade onset among input-input pairs. Because the timing of this drop
176 precedes saccadic initiation, which begins ~ 150 ms before saccade onset^{46,47}, it could not be the
177 result of a corollary discharge signal. Instead, it may reflect the shift in internal state that occurs
178 before saccadic initiation as the subject shifts their attention towards a potential target location⁴⁸.
179 In accordance with this possibility, pupil diameter, a well-established correlate of internal state^{49,50},
180 begins to ramp several hundred milliseconds prior to saccade onset (Figure S4B)⁵¹. Similar shifts
181 in internal state are known to be accompanied by comparable reductions in correlated
182 variability^{50,52-54}.

183 To further characterize changes in coordinated peri-saccadic activity, we also examined
184 differences in spike-spike coherence (SSC) before and after saccade onset. Spike-spike coherence
185 is a measure of the degree to which the activity of two signals, in this case a pair of simultaneously
186 recorded single- and/or multi-units, fluctuates together across a range of frequencies. We found
187 that saccade onset increases wide-band coherence most prominently in the input layer, with
188 weaker, but still significant, effects in the superficial and deep layers (Figure 4C). When quantified
189 as a modulation index (Figure 4D), we observed significant modulation in all layers at all
190 frequencies, with the exception of the 30-100 Hz band in the superficial layer. The input layer
191 exhibits larger increases in coherence, particularly at higher frequencies, while the deep layer
192 experiences smaller increases, particularly at lower frequencies. Collectively, these data suggest
193 that saccade onset leads to a temporary elevation of correlated activity, which manifests itself most
194 prominently in the input layer. The timing and magnitude of changes in correlated variability,
195 measured with both SCC and SSC, further suggests that an external signal arrives prior to saccade
196 onset within the input layer before then propagating to the other layers.

197

198 **Saccades Increase the Strength of Low-Frequency Wide-Band Activity**

199 Increases in coordinated activity at the level of single neurons can result in an elevation of
200 population-level wide-band activity. To determine whether this held true for saccades, we
201 calculated the spectral power, a frequency-resolved measure of signal strength, of the LFP around
202 the time of saccade onset. Saccade onset was associated with a large elevation in low frequency
203 power, and a slight reduction in high frequency power (Figure 5A). Comparing the power spectrum
204 before and after saccade onset, we found that these differences were significant in all three
205 frequency bands tested, with an elevation in the 0-12 Hz and 15-25 Hz bands and a reduction in

206 the 30-80 Hz band after saccade onset (Figure 5B). Next, we sought to investigate whether the
207 increased strength of low-frequency wide-band activity entrains spiking units, as reported
208 previously in other contexts⁵⁵⁻⁵⁷. We found that saccade onset significantly increases low-
209 frequency spike-LFP phase locking (Figure 5C), as measured by pairwise phase consistency
210 (PPC). These results indicate that saccade onset increases the strength of population-level low-
211 frequency wide-band activity, which could in turn entrain the activity of local neurons.

212

213 **A Computational Model Demonstrates that Activation of an Input Layer-Targeting** 214 **Projection is Sufficient for Inducing Saccadic Suppression**

215 Given that input layer units exhibit significant changes in firing properties prior to saccade onset,
216 we hypothesized that a projection targeting this layer could serve as the initiator of saccadic
217 suppression within area V4. To determine whether such a projection would be sufficient for
218 initiating suppression across all cortical layers, as well as to gain further insight into the associated
219 circuit-level mechanisms, we developed a computational model of peri-saccadic activity changes
220 within a cortical column. Our model draws inspiration from previous cortical circuit models that
221 describe population-specific firing rate changes in response to the activation of an external input⁵⁸.
222 To more faithfully simulate cortical circuit-level dynamics, our model consists of six
223 interconnected populations across three layers of the cortex (Figure 6A, left). Each cortical layer
224 contains an excitatory (E) and inhibitory (I) population, which project to each other as well as to
225 themselves. Given evidence of multiple operating regimes for a local E-I network in the visual
226 cortex, connections within a layer were tuned to allow the local E-I network to switch in and out
227 of an inhibition-stabilized network (ISN) regime^{59,60}: the baseline regime of the network is non-
228 ISN, but direct external input to the E population switches it to ISN (see Methods; Figure S5A-C).

229 Connections between layers exist in the form of projections from E neurons in the source layer to
230 both E and I neurons in the target layer, with E-E and E-I connections tuned to affect a net increase
231 in E activity in the target layer in response to an increase in E activity in the source layer. In our
232 model, the input layer projects to the superficial layer, which then projects to the deep layer; this
233 connectivity motif highlights the primary pathway for information flow within a visual cortical
234 column^{13,61}. In light of our empirical firing rate analysis, which found that both broad- and narrow-
235 spiking units in the input layer show responses prior to saccade onset (Figure 3B), we chose to
236 model the input layer as the primary recipient of the ‘saccadic signal’ input. We tuned the strength
237 of the excitatory ‘saccadic signal’ pathway to the local E and I populations in this layer such that
238 its activation affected a net suppression of the E activity.

239 In response to the activation of a saccadic signal of sufficient strength slightly before the
240 time of saccade onset, the E input layer population rate was suppressed. In addition, our model
241 simultaneously recapitulated our experimental findings in the input layer I population
242 (enhancement), as well as the E/I populations in other layers (suppression) by virtue of the inter-
243 and intra-layer connectivity (Figure 6B, S5B). Since local E activity is a major source of excitation
244 to the I population within a layer, we next explored the role of the saccadic signal in sustaining
245 input layer I activity despite a concurrent decline in local E activity. We explored three scenarios
246 with saccadic signals of varying magnitudes ramping up and down over a fixed period (Figure 6C,
247 top). We found that the increase in I activity in the input layer indeed depended on the strength of
248 the saccadic signal and was sustained at sufficiently high magnitudes. Examination of the
249 contribution of different excitatory pathways to the I population showed that sufficiently high
250 saccadic signal magnitude led to an increase in net excitation onto the I population that exceeded
251 the loss in excitation resulting from the reduction of local E firing rates (Figure 6C, middle and

252 bottom). Our model thus demonstrates that an input layer-specific saccadic signal of adequate
253 strength can increase local I activity, which is sufficient for inducing suppression across the depth
254 of the cortex. These findings correspond closely to our empirical observations. The model further
255 predicted that the time course of the increase in input layer I activity was dependent on the baseline
256 operating regime of the E-I network. When the network was robustly within the non-*ISN* regime,
257 I activity increased immediately following saccadic signal onset. However, when the network was
258 close to the switching point between the two regimes, the I activity showed little change below a
259 saccadic signal of sufficient magnitude, even when the local E activity showed significant
260 suppression (Figure S5E). This latter scenario corresponds closely to our empirical observations
261 in the input layer (Figure 2B-C), suggesting that the baseline state of the cortical network lies close
262 to the boundary between regimes.

263 Our experimental paradigm examined peri-saccadic cortical dynamics in the absence of
264 visual input. While this allowed us to investigate the cortical dynamics that are purely a result of
265 the saccadic signal and avoid potential stimulus-induced artifacts in our recordings, it leaves open
266 the question of how activity patterns might change in the presence of visual stimulation. To explore
267 this further, we added a second external excitatory input ('visual signal') to the input layer E
268 population (Figure 6A, right), which is the major target of feedforward visual input into V4¹⁴. The
269 addition of this second input shifted the local E-I network into an *ISN* regime⁵⁹, in which E and I
270 activity increase or decrease concurrently. As a result, simultaneous activation of the visual signal
271 led to a net reduction in the firing rate of both E and I input layer populations (Figure 6D, S5C).
272 This produced a similar reduction in excitatory drive to the superficial and deep layers, where
273 firing was again suppressed. These results are consistent with prior reports of suppression from
274 uncategorized neurons in the visual cortex in the presence of visual stimulation^{3,5,6}.

275 **DISCUSSION**

276 Our results provide evidence that the input layer of area V4 receives the earliest information about
277 upcoming saccades. Units in the input layer showed changes in firing rate prior to saccade onset,
278 while units in other layers did not. In addition, elevated spike-count correlations, a common
279 byproduct of activating a shared input to a neural population⁶²⁻⁶⁵, were observed earliest among
280 pairs of input layer neurons. Consistent with a single input source (i.e. projection) producing both
281 phenomena, changes in the firing rate and correlational structure of input layer units were initiated
282 with similar timing, approximately 40 ms before saccade onset. These convergent results indicate
283 that the saccadic signaling pathway in question predominantly targets the input layer, which
284 thereby allows us to infer its source. Given the lack of pre-saccadic modulation in the superficial
285 and deep layers, it is unlikely that a projection from the FEF is responsible for the observed
286 suppression. Likewise, it is doubtful that suppression is fed forward by projections from lower
287 visual areas (V1/V2/V3), as such a mechanism would not explain the enhancement of narrow-
288 spiking input layer firing rates in V4. Furthermore, to our knowledge, there have been no clear
289 reports of saccadic suppression in V2 or V3, and while V1 is known to be suppressed during
290 saccades, it does not exhibit pre-saccadic modulation²⁶, and could therefore not be responsible for
291 the changes in activity described here. Thus, we propose that saccadic suppression in V4 is likely
292 initiated via thalamo-cortical projections from the pulvinar.

293 Several lines of research are consistent with this view. Peri-saccadic modulation has been
294 observed in the pulvinar of macaques, where neurons respond to saccades made in the dark without
295 visual stimulation^{32,33}. Neurons in the pulvinar of cats are able to distinguish between internally
296 generated saccades and simulated saccades produced with image motion, demonstrating that they
297 encode the underlying motor command³¹. Furthermore, the pulvinar is known to play a crucial role

298 in spatial attention⁶⁶⁻⁶⁸, which is necessary for the proper execution of saccades towards target
299 stimuli; indeed, temporary inactivation of the pulvinar results in significant deficits in saccadic
300 target selection and execution^{69,70}. These findings indicate that neurons in the pulvinar would be
301 able to provide a meaningful saccadic signal to their efferent targets.

302 We also found that narrow-spiking units in the input layer showed a peri-saccadic
303 enhancement in firing. Narrow-spiking units are thought to correspond to parvalbumin-expressing
304 inhibitory interneurons^{71,72}, and are known to receive strong thalamocortical excitation.⁷³⁻⁷⁵ This
305 led us to speculate that an elevated level of inhibition within the input layer could suppress local
306 excitatory neurons, as well as neurons in other cortical layers (Figure 6A). To explore this
307 hypothesis, we developed a six-population firing rate model of the visual cortex and its modulation
308 during saccades. The model demonstrated that pre-saccadic activation of an input layer-targeting
309 projection is sufficient for suppressing signaling within a cortical column. A compelling aspect of
310 our model is its simplicity – with straightforward inter-population connectivity rules, we were able
311 to both replicate our empirical findings as well as reconcile the opposing patterns of activity
312 observed in the input layer subpopulations. The model also reproduces trends in our experimental
313 observations on the relative time course of broad and narrow spiking activity under a set of
314 conditions wherein the input layer operates on the cusp of ISN and non-ISN operating regimes.
315 Given these results, we propose that inhibitory input layer neurons initiate saccadic suppression
316 and gate the processing of visual information entering the local cortical network.

317 We also observed increases in correlated activity across all cortical layers during saccades,
318 in the form of elevated spike-count correlations, spike-spike coherence, low-frequency power, and
319 low frequency spike-phase locking. Comparable increases in neural correlation have been
320 associated with diminished stimulus sensitivity in multiple model organisms across a variety of

321 sensory modalities^{50,76-79}. This may be a result of heightened correlations functionally limiting the
322 ability of a neural population to encode information, as suggested by previous experimental and
323 theoretical work⁸⁰⁻⁸³. Similarly, saccadic suppression at the level of neurons and circuits is also
324 accompanied by a behaviorally significant reduction in stimulus detection capabilities^{1,2},
325 indicating that the increases in correlated variability reported here may reflect or contribute to that
326 deficit.

327 In summary, we conclude that an input layer-targeting projection, likely originating in the
328 pulvinar, initiates saccadic suppression within V4 by enhancing the firing of local inhibitory
329 interneurons. Future work could extend this line of subpopulation-specific, circuit-level analysis
330 to examine activity changes during saccades in the presence of visual stimulation. Our model
331 provides a prediction for such experiments, suggesting that the peri-saccadic activity of inhibitory
332 input layer neurons would also be suppressed when the cortex is in a state of active information
333 processing. The absence of any reports of subpopulation-specific differences in peri-saccadic
334 modulation during previous studies employing cued saccade tasks is consistent with this view.

335 **METHODS**

336 **Surgical Procedures**

337 Surgical procedures have been described in detail previously^{84,85}. In brief, an MRI-
338 compatible, low-profile titanium chamber was placed over the pre-lunate gyrus on the basis of
339 preoperative MRI imaging in two rhesus macaques (right hemisphere in monkey A, left
340 hemisphere in monkey C). The native dura mater was then removed, and a silicone-based, optically
341 clear artificial dura (AD) was inserted, resulting in an optical window over dorsal V4. All
342 procedures were approved by the Institutional Animal Care and Use Committee and conformed to
343 NIH guidelines.

344 **Electrophysiology**

345 At the beginning of each recording session, a plastic insert with an opening for targeting
346 electrodes was lowered into the chamber and secured. This served to stabilize the recording site
347 against cardiac pulsations. Neurons were recorded from cortical columns in dorsal V4 using 16-
348 channel linear array electrodes (“laminar probes”; Plexon, Plexon V-probe). The laminar probes
349 were mounted on adjustable x-y stages attached to the recording chamber and positioned over the
350 center of the pre-lunate gyrus under visual guidance through a microscope (Zeiss). This ensured
351 that the probes were maximally perpendicular to the surface of the cortex and thus had the best
352 possible trajectory to make a normal penetration down a cortical column. Across recording
353 sessions, the probes were positioned over different sites along the center of the gyrus in the
354 parafoveal region of V4 with receptive field eccentricities between 2 and 7 degrees of visual angle.
355 Care was taken to target cortical sites with no surface micro-vasculature and, in fact, the surface
356 micro-vasculature was used as reference so that the same cortical site was not targeted across
357 recording sessions. The probes were advanced using a hydraulic microdrive (Narishige) to first

358 penetrate the AD and then through the cortex under microscopic visual guidance. Probes were
359 advanced until the point that the top-most electrode (toward the pial surface) registered LFP
360 signals. At this point, the probe was retracted by about 100–200 μm to ease the dimpling of the
361 cortex due to the penetration. This procedure greatly increased the stability of the recordings and
362 also increased the neuronal yield in the superficial electrodes.

363 The distance from the tip of the probes to the first electrode contact was either 300 μm or
364 700 μm . The inter-electrode distance was 150 μm , thus negating the possibility of recording the
365 same neural spikes in adjacent recording channels. Neuronal signals were recorded extra-
366 cellularly, filtered, and stored using the Multi-channel Acquisition Processor system (Plexon).
367 Neuronal signals were classified as either multi-unit clusters or isolated single-units using the
368 Plexon Offline Sorter program. Single-units were identified based on two criteria: (1) if they
369 formed an identifiable cluster, separate from noise and other units, when projected into the
370 principal components of waveforms recorded on that electrode and (2) if the inter-spike interval
371 (ISI) distribution had a well-defined refractory period. Single-units were classified as either
372 narrow-spiking (putative interneurons) or broad-spiking (putative pyramidal cells) based on
373 methods described in detail previously⁴¹. Specifically, only units with waveforms having a clearly
374 defined peak preceded by a trough were potential candidates. Units with trough-to-peak duration
375 less than 225 ms were classified as narrow-spiking units; units with trough- to-peak duration
376 greater than 225 ms were classified as broad-spiking units.

377 Data were collected over 17 sessions (8 sessions in monkey A and 9 in monkey C), yielding
378 a total of 211 single-units (99 narrow-spiking, 112 broad-spiking) and 110 multi-unit clusters.

379 **Recording**

380 Stimuli were presented on a computer monitor placed 57 cm from the eye. Eye position
381 was continuously monitored with an infrared eye tracking system (ISCAN ETL-200). Trials were
382 aborted if eye position deviated more than 1 degree of visual angle from fixation. Experimental
383 control was handled by NIMH Cortex software (<http://www.cortex.salk.edu/>).

384 ***Receptive Field Mapping***

385 At the beginning of each recording session, neuronal RFs were mapped using subspace
386 reverse correlation in which Gabor (eight orientations, 80% luminance contrast, spatial frequency
387 1.2 cycles/degree, Gaussian half-width 2 degrees) or ring (80% luminance contrast) stimuli
388 appeared at 60 Hz while monkeys fixated. Each stimulus appeared at a random location selected
389 from an 11 x 11 grid with 1 degree spacing in the appropriate visual quadrant. Spatial receptive
390 maps were obtained by applying reverse correlation to the evoked LFP signal at each recording
391 site. For each spatial location in the 11 x 11 grid, we calculated the time-averaged power in the
392 stimulus-evoked LFP (0–200 ms after each stimulus flash) at each recording site. The resulting
393 spatial map of LFP power was taken as the spatial RF at the recording site. For the purpose of
394 visualization, the spatial RF maps were smoothed using spline interpolation and displayed as
395 stacked contours plots of the smoothed maps (Figure 1B). All RFs were in the lower visual
396 quadrant (lower left in monkey A and lower right in monkey C) and with eccentricities between 2
397 and 7 degrees of visual angle.

398 ***Current Source Density Mapping***

399 In order to estimate the laminar identity of each recording channel, we used a CSD mapping
400 procedure³⁹. Monkeys maintained fixation while 100% luminance contrast ring stimuli were
401 flashed (30 ms), centered at the estimated RF overlap region across all channels. The size of the
402 ring was scaled to about three-quarters of the estimated diameter of the RF. CSD was calculated

403 as the second spatial derivative of the flash-triggered LFPs. The resulting time-varying traces of
404 current across the cortical layers can be visualized as CSD maps (Figure 1C). Red regions depict
405 current sinks in the corresponding region of the cortical laminae; blue regions depict current
406 sources. The input layer (Layer 4) was identified as the first current sink followed by a reversal to
407 current source. The superficial (Layers 1–3) and deep (Layers 5 and 6) layers had opposite sink-
408 source patterns. LFPs and spikes from the corresponding recording channels were then assigned
409 to one of three layers: superficial, input, or deep.

410 *Spontaneous Recordings*

411 In the main experiment, all monitors and lights were turned off in the recording room and
412 adjacent control room to ensure that the environment was as dark as experimentally feasible. Eye
413 tracker and electrophysiological data were recorded while the animals executed eye-movements
414 freely in the dark.

415 **Data Analysis**

416 *Saccade Identification*

417 To identify saccade onset and offset times from the raw eye-tracker data, we used the
418 Cluster Fix algorithm⁸⁶. Cluster Fix performs k-means clustering on four parameters (distance,
419 velocity, acceleration, and angular velocity) to find natural partitions in the eye-tracker data and
420 identify saccades. To ensure that our set of identified eye movements was ‘clean,’ we imposed
421 several additional criteria: 1) to avoid adjacent saccades affecting our analysis, we only considered
422 saccades separated from neighboring saccades by at least 500 ms, 2) to exclude microsaccades, we
423 only considered saccades that were greater in amplitude than 0.7 degrees of visual angle, 3) to
424 exclude slower eye movements that Cluster Fix had mislabeled as saccades, we only considered
425 eye movements less than 200 ms in duration, and 4) to exclude periods of data erroneously labeled

426 as saccades due to blinking or drowsiness, we identified those periods using pupil diameter
427 measurements and excluded nearby saccades.

428 Saccadic eye movements are known to have an approximately linear relationship between
429 amplitude and peak velocity that is referred to as the main sequence³⁸. To ensure that our approach
430 identified a set of eye movements that quantitatively resembled the properties of saccades, we
431 calculated the amplitude and peak velocity for each of the identified eye movements and found an
432 approximately linear relationship (Figure 1A).

433 *Firing Rate Estimation and Modulation Index*

434 To estimate the peri-saccadic firing rate, spikes were extracted for each saccade beginning
435 500 ms prior to saccade onset and ending 500 ms after saccade onset. To obtain a continuous
436 estimate of the firing rate, each spike was convolved with a gaussian kernel and the average firing
437 rate across saccades was calculated for each unit (Figure S1; Figure S2). The kernel bandwidth
438 was selected on a unit-by-unit basis at each point in time using a bandwidth optimization algorithm
439 that minimized the mean integrated squared error⁴⁵. In order to obtain reliable firing rate estimates,
440 only units that fired at least 75 spikes within 500 ms of saccade onset (before or after) were
441 included.

442 A modulation index was calculated for each unit to estimate the degree to which their
443 activity deviated from baseline following saccade onset (Figure 2D, E; Figure S3). The modulation
444 index was defined as $FR_s/FR_b - FR_b$, where FR_s is the maximum firing rate in the 200 ms after
445 saccade onset and FR_b is the baseline firing rate of the unit, calculated by averaging the firing rate
446 for each unit in a time window 350 to 250 ms before saccade onset.

447 *Spike Count Correlations*

448 To obtain a continuous estimate of spike count correlations, we calculated the Pearson
449 correlation of spike counts across saccades at each time bin for every pair of simultaneously
450 recorded single- and multi-units (Figure 4A, Figure S4A). The time window was 201 ms in width,
451 and was shifted by 1 ms steps. Spike counts were z-scored to control for firing rate differences
452 across time. Traces were smoothed with a 101 ms Gaussian weighted moving average. To perform
453 the timing analysis, we took the local minimum in correlation as the time at which the rise begins.
454 Bootstrapping was performed for each pair type to obtain confidence intervals on the estimate
455 (Figure 4B).

456 *Spike-Spike Coherence*

457 We computed the coherence between simultaneously recorded, multi-unit pairs within a
458 cortical layer using multi-taper methods⁸⁷ for two different windows: the 200 ms before and after
459 saccade onset (Figure 4C). Spike trains were tapered with a single Slepian taper (TW = 3, K = 5).
460 Magnitude of coherence estimates depend on the number of spikes used to create the estimates⁸⁸.
461 To control for differences in firing rate across the two windows, we adopted a rate-matching
462 procedure⁵³. In order to obtain a baseline for the coherence expected solely due to trends in firing
463 time-locked to saccade onset, we also computed coherence in which saccade identities were
464 randomly shuffled. Only units that elicited at least 50 spikes from each neuron cumulatively across
465 all saccades in both time windows were considered. A modulation index, defined as
466 $(SSC_{after} - SSC_{before}) / (SSC_{after} + SSC_{before})$, was calculated for each pair of units at each
467 frequency band (Figure 4D).

468 *Power*

469 Local field potential power was calculated with multi-tapered methods⁸⁷. Signals were
470 tapered with a single Slepian taper (TW = 3, K = 5). Spectrograms (Figure 5A) were generated by

471 sliding a 201 ms window by increments of 1 ms. Power spectra before (-200 to 0 ms) and after (0
472 to 200 ms) saccade onset were calculated with static variants of the same methods (Figure 5B). No
473 layer-specific differences were found, so results shown here are averaged across all recording
474 channels.

475 *Pairwise Phase Consistency*

476 The pairwise phase consistency (PPC) is an estimate of spike-field locking that is not
477 biased by spike count or firing rate⁸⁹. Two segments of data were analyzed: the 200 ms before and
478 after saccade onset. In order to obtain reliable estimates, only units that fired at least 50 spikes
479 cumulatively across all saccades during both time windows were considered. The spectro-temporal
480 representation of the local field potential signal was generated through a continuous wavelet
481 transform with a family of complex Morlet wavelets (spanning frequencies from 2 to 100 Hz, with
482 6 cycles at each frequency). Phase information was extracted at the time of each spike, and the
483 PPC was then calculated for each unit with each LFP channel in the laminar probes (Figure 5C).
484 We observed minimal change in the PPC as a function of LFP layer, so the results presented here
485 were averaged across all recording channels.

486 *Computational Model*

487 The firing rate or mean field model consists of a network of six populations representing
488 excitatory (E) and inhibitory (I) populations in the superficial (L1), input (L2), and deep (L3) layers
489 of the cortex. The firing rate model describes temporal changes in the firing rates (r) of each
490 population as a function of the activity of two external inputs (i_{sacc} , the saccadic signal, and i_{stim} ,
491 the visual signal) and the activity of other populations in the network. The connectivity between
492 populations is depicted in Figure 6A. The network consists of a coupled E-I network in each layer
493 and captures the core aspect of connectivity between cortical layers: information flow from input

494 to superficial to deep layer. The saccadic signal is sent to both E and I populations in the input
 495 layer, while the visual signal is sent only to the E population in the input layer. The saccadic signal
 496 is described by a ramping function (Figure 6C, top). The visual signal is only activated in the
 497 second set of simulations, where it is held constant to replicate sustained visual input. The six-
 498 population rate model is described by the following equations:

$$499 \quad \tau_E \frac{dr_{EL1}}{dt} = -r_{EL1} + G_E(W_{EE} \cdot r_{EL1} - W_{EI} \cdot r_{IL1} + W_{EEL12} \cdot r_{EL2}) \quad (1)$$

$$500 \quad \tau_I \frac{dr_{IL1}}{dt} = -r_{IL1} + G_I(W_{IE} \cdot r_{EL1} - W_{II} \cdot r_{IL1} + W_{IEL12} \cdot r_{EL2}) \quad (2)$$

$$501 \quad \tau_E \frac{dr_{EL2}}{dt} = -r_{EL2} + G_E(W_{EE} \cdot r_{EL2} - W_{EI} \cdot r_{IL2} + W_{EESS} \cdot i_{sacc} + i_{stim}) \quad (3)$$

$$502 \quad \tau_I \frac{dr_{IL2}}{dt} = -r_{IL2} + G_I(W_{IE} \cdot r_{EL2} - W_{II} \cdot r_{IL2} + W_{IESS} \cdot i_{sacc}) \quad (4)$$

$$503 \quad \tau_E \frac{dr_{EL3}}{dt} = -r_{EL3} + G_E(W_{EE} \cdot r_{EL3} - W_{EI} \cdot r_{IL3} + W_{EEL32} \cdot r_{EL1}) \quad (5)$$

$$504 \quad \tau_I \frac{dr_{IL3}}{dt} = -r_{IL3} + G_I(W_{IE} \cdot r_{EL3} - W_{II} \cdot r_{IL3} + W_{IEL32} \cdot r_{EL1}) \quad (6)$$

$$505 \quad G(x) = \begin{cases} 0 & \text{for } x < \theta \\ m(x - \theta)^{2.5} & \text{for } \theta < x < \theta + 1/m \\ 1 & \text{for } x > \theta + 1/m \end{cases} \quad (7)$$

506 τ_E and τ_I are the rates at which the excitatory and inhibitory populations approach their steady
 507 states. G_E and G_I are the population response functions, described by equation (7), for the
 508 excitatory and inhibitory populations that transform the given inputs into a firing response. θ is
 509 the threshold input and m is the rate of the response function. Parameters tuned in the model to
 510 recapitulate the population level observations in experimental data: $W_{EE} = 25$, $W_{II} = 4$, $W_{EI} =$
 511 25 , $W_{IE} = 20$, $W_{EEL12} = 20$, $W_{IEL12} = 2$, $W_{EESS} = 0.5$, $W_{IESS} = 3$, $W_{EEL32} = 30$, $W_{IEL32} = 4$, $\tau_E =$

512 $0.008, \tau_I = 0.004, m_E = 0.001, m_I = 0.005, \theta_{E_{L1}} = -3, \theta_{E_{L2}} = -5, \theta_{E_{L3}} = -5, \theta_{I_{L1}} = 0,$
513 $\theta_{I_{L2}} = 8, \theta_{I_{L3}} = 8, i_{stim} = 10.$

514 A further tuning was applied to the model to switch each E-I population between an
515 inhibitory stabilized network (ISN) regime and a non-ISN one⁶⁰. Experimental data from visual
516 cortex suggest that a cortical network switches to an ISN regime during stimulus processing⁵⁹,
517 hence we included this feature to generate model predictions for saccadic suppression-related
518 laminar activity during stimulus presentation. Previous modeling work has shown that a firing-
519 rate E-I network model can switch between these regimes either by modification of connection
520 weights (W), change in slope or rate of response functions (m) or a combination of both⁶⁰. We
521 implemented the simplest mechanism for the network to switch between ISN and non-ISN
522 regime: nonlinear response functions. When visual stimulation (modeled as an excitatory input to
523 the input layer E population) is applied to the model cortical column, the network moves to a
524 higher slope region of its response functions, and switches to the ISN operating regime. A
525 phase-plane analysis of the E-I network model illustrates how this results in a distinct response
526 of the network to exactly the same saccadic signal input (Figure S5).

527

528 **ACKNOWLEDGEMENTS**

529 This research was supported by NIH R01 EY021827 to JHR and ASN, NARSAD Young
530 Investigator Grant, Ziegler Foundation Grant and Yale Orthwein Scholar Funds to ASN, NIH
531 R00 EY025026 to MPJ, and by NEI core grants for vision research P30 EY019005 to the Salk
532 Institute and P30 EY026878 to Yale University. We would like to thank Catherine Williams and
533 Mat LeBlanc for excellent animal care.

534

535 **AUTHOR CONTRIBUTIONS**

536 SD & ASN conceptualized the project. ASN collected the data and supervised the project. SD
537 analyzed the data, with assistance from MPM and ASN. MPJ developed the computational model.
538 SD, ASN, MPJ, and JHR wrote the manuscript.

539

540 **COMPETING INTERESTS**

541 The authors declare no competing interests.

542 **REFERENCES**

- 543 1 Matin, E. Saccadic suppression: a review and an analysis. *Psychol Bull* **81**, 899-917,
544 doi:10.1037/h0037368 (1974).
- 545 2 Zuber, B. L. & Stark, L. Saccadic suppression: elevation of visual threshold associated
546 with saccadic eye movements. *Exp Neurol* **16**, 65-79, doi:10.1016/0014-4886(66)90087-2
547 (1966).
- 548 3 Thiele, A., Henning, P., Kubischik, M. & Hoffmann, K. P. Neural mechanisms of saccadic
549 suppression. *Science* **295**, 2460-2462, doi:10.1126/science.1068788 (2002).
- 550 4 Kleiser, R., Seitz, R. J. & Krekelberg, B. Neural correlates of saccadic suppression in
551 humans. *Curr Biol* **14**, 386-390, doi:10.1016/j.cub.2004.02.036 (2004).
- 552 5 Bremmer, F., Kubischik, M., Hoffmann, K. P. & Krekelberg, B. Neural dynamics of
553 saccadic suppression. *J Neurosci* **29**, 12374-12383, doi:10.1523/JNEUROSCI.2908-
554 09.2009 (2009).
- 555 6 Zanos, T. P., Mineault, P. J., Guitton, D. & Pack, C. C. Mechanisms of Saccadic
556 Suppression in Primate Cortical Area V4. *J Neurosci* **36**, 9227-9239,
557 doi:10.1523/JNEUROSCI.1015-16.2016 (2016).
- 558 7 Wurtz, R. H., Joiner, W. M. & Berman, R. A. Neuronal mechanisms for visual stability:
559 progress and problems. *Philos Trans R Soc Lond B Biol Sci* **366**, 492-503,
560 doi:10.1098/rstb.2010.0186 (2011).
- 561 8 Sommer, M. A. & Wurtz, R. H. A pathway in primate brain for internal monitoring of
562 movements. *Science* **296**, 1480-1482, doi:10.1126/science.1069590 (2002).
- 563 9 Sommer, M. A. & Wurtz, R. H. Influence of the thalamus on spatial visual processing in
564 frontal cortex. *Nature* **444**, 374-377, doi:10.1038/nature05279 (2006).
- 565 10 Roe, A. W. *et al.* Toward a unified theory of visual area V4. *Neuron* **74**, 12-29,
566 doi:10.1016/j.neuron.2012.03.011 (2012).
- 567 11 Han, X., Xian, S. X. & Moore, T. Dynamic sensitivity of area V4 neurons during saccade
568 preparation. *Proc Natl Acad Sci U S A* **106**, 13046-13051, doi:10.1073/pnas.0902412106
569 (2009).
- 570 12 Hirsch, J. A. & Martinez, L. M. Laminar processing in the visual cortical column. *Curr*
571 *Opin Neurobiol* **16**, 377-384, doi:10.1016/j.conb.2006.06.014 (2006).
- 572 13 Douglas, R. J. & Martin, K. A. Neuronal circuits of the neocortex. *Annu Rev Neurosci* **27**,
573 419-451, doi:10.1146/annurev.neuro.27.070203.144152 (2004).
- 574 14 Felleman, D. J. & Van Essen, D. C. in *Cereb cortex*. (Citeseer).

- 575 15 Ungerleider, L. G., Galkin, T. W., Desimone, R. & Gattass, R. Cortical connections of area
576 V4 in the macaque. *Cereb Cortex* **18**, 477-499, doi:10.1093/cercor/bhm061 (2008).
- 577 16 Rockland, K. S. & Pandya, D. N. Laminar origins and terminations of cortical connections
578 of the occipital lobe in the rhesus monkey. *Brain Res* **179**, 3-20, doi:10.1016/0006-
579 8993(79)90485-2 (1979).
- 580 17 Boussaoud, D., Ungerleider, L. G. & Desimone, R. Pathways for motion analysis: cortical
581 connections of the medial superior temporal and fundus of the superior temporal visual
582 areas in the macaque. *J Comp Neurol* **296**, 462-495, doi:10.1002/cne.902960311 (1990).
- 583 18 Distler, C., Boussaoud, D., Desimone, R. & Ungerleider, L. G. Cortical connections of
584 inferior temporal area TEO in macaque monkeys. *J Comp Neurol* **334**, 125-150,
585 doi:10.1002/cne.903340111 (1993).
- 586 19 Borra, E., Ichinohe, N., Sato, T., Tanifuji, M. & Rockland, K. S. Cortical connections to
587 area TE in monkey: hybrid modular and distributed organization. *Cereb Cortex* **20**, 257-
588 270, doi:10.1093/cercor/bhp096 (2010).
- 589 20 Gattass, R., Galkin, T. W., Desimone, R. & Ungerleider, L. G. Subcortical connections of
590 area V4 in the macaque. *J Comp Neurol* **522**, 1941-1965, doi:10.1002/cne.23513 (2014).
- 591 21 Anderson, J. C., Kennedy, H. & Martin, K. A. Pathways of attention: synaptic relationships
592 of frontal eye field to V4, lateral intraparietal cortex, and area 46 in macaque monkey. *J*
593 *Neurosci* **31**, 10872-10881, doi:10.1523/JNEUROSCI.0622-11.2011 (2011).
- 594 22 Stanton, G. B., Bruce, C. J. & Goldberg, M. E. Topography of projections to posterior
595 cortical areas from the macaque frontal eye fields. *J Comp Neurol* **353**, 291-305,
596 doi:10.1002/cne.903530210 (1995).
- 597 23 Benevento, L. A. & Rezak, M. The cortical projections of the inferior pulvinar and adjacent
598 lateral pulvinar in the rhesus monkey (*Macaca mulatta*): an autoradiographic study. *Brain*
599 *Res* **108**, 1-24, doi:10.1016/0006-8993(76)90160-8 (1976).
- 600 24 Shipp, S. The functional logic of cortico-pulvinar connections. *Philos Trans R Soc Lond B*
601 *Biol Sci* **358**, 1605-1624, doi:10.1098/rstb.2002.1213 (2003).
- 602 25 Rockland, K. S. Distinctive Spatial and Laminar Organization of Single Axons from
603 Lateral Pulvinar in the Macaque. *Vision* **4**, 1 (2020).
- 604 26 McFarland, J. M., Bondy, A. G., Saunders, R. C., Cumming, B. G. & Butts, D. A. Saccadic
605 modulation of stimulus processing in primary visual cortex. *Nat Commun* **6**, 8110,
606 doi:10.1038/ncomms9110 (2015).
- 607 27 Wurtz, R. H. Response of striate cortex neurons to stimuli during rapid eye movements in
608 the monkey. *J Neurophysiol* **32**, 975-986, doi:10.1152/jn.1969.32.6.975 (1969).

- 609 28 Bizzi, E. Discharge of frontal eye field neurons during saccadic and following eye
610 movements in unanesthetized monkeys. *Exp Brain Res* **6**, 69-80, doi:10.1007/BF00235447
611 (1968).
- 612 29 Schall, J. D. & Hanes, D. P. Neural basis of saccade target selection in frontal eye field
613 during visual search. *Nature* **366**, 467-469, doi:10.1038/366467a0 (1993).
- 614 30 Everling, S. & Munoz, D. P. Neuronal correlates for preparatory set associated with pro-
615 saccades and anti-saccades in the primate frontal eye field. *J Neurosci* **20**, 387-400 (2000).
- 616 31 Robinson, D. L., McClurkin, J. W., Kertzman, C. & Petersen, S. E. Visual responses of
617 pulvinar and collicular neurons during eye movements of awake, trained macaques. *J*
618 *Neurophysiol* **66**, 485-496, doi:10.1152/jn.1991.66.2.485 (1991).
- 619 32 Berman, R. A. & Wurtz, R. H. Signals conveyed in the pulvinar pathway from superior
620 colliculus to cortical area MT. *J Neurosci* **31**, 373-384, doi:10.1523/JNEUROSCI.4738-
621 10.2011 (2011).
- 622 33 Sudkamp, S. & Schmidt, M. Response characteristics of neurons in the pulvinar of awake
623 cats to saccades and to visual stimulation. *Exp Brain Res* **133**, 209-218,
624 doi:10.1007/s002210000374 (2000).
- 625 34 Katzner, S., Busse, L. & Carandini, M. GABAA inhibition controls response gain in visual
626 cortex. *J Neurosci* **31**, 5931-5941, doi:10.1523/JNEUROSCI.5753-10.2011 (2011).
- 627 35 Wilson, N. R., Runyan, C. A., Wang, F. L. & Sur, M. Division and subtraction by distinct
628 cortical inhibitory networks in vivo. *Nature* **488**, 343-348, doi:10.1038/nature11347
629 (2012).
- 630 36 Mitchell, S. J. & Silver, R. A. Shunting inhibition modulates neuronal gain during synaptic
631 excitation. *Neuron* **38**, 433-445, doi:10.1016/s0896-6273(03)00200-9 (2003).
- 632 37 Berman, R. A., Cavanaugh, J., McAlonan, K. & Wurtz, R. H. A circuit for saccadic
633 suppression in the primate brain. *J Neurophysiol* **117**, 1720-1735,
634 doi:10.1152/jn.00679.2016 (2017).
- 635 38 Bahill, A. T., Clark, M. R. & Stark, L. The main sequence, a tool for studying human eye
636 movements. *Mathematical Biosciences* **24**, 191-204 (1975).
- 637 39 Mitzdorf, U. Current source-density method and application in cat cerebral cortex:
638 investigation of evoked potentials and EEG phenomena. *Physiol Rev* **65**, 37-100,
639 doi:10.1152/physrev.1985.65.1.37 (1985).
- 640 40 Nandy, A. S., Nassi, J. J. & Reynolds, J. H. Laminar Organization of Attentional
641 Modulation in Macaque Visual Area V4. *Neuron* **93**, 235-246,
642 doi:10.1016/j.neuron.2016.11.029 (2017).

- 643 41 Mitchell, J. F., Sundberg, K. A. & Reynolds, J. H. Differential attention-dependent
644 response modulation across cell classes in macaque visual area V4. *Neuron* **55**, 131-141,
645 doi:10.1016/j.neuron.2007.06.018 (2007).
- 646 42 Tamura, H., Kaneko, H., Kawasaki, K. & Fujita, I. Presumed inhibitory neurons in the
647 macaque inferior temporal cortex: visual response properties and functional interactions
648 with adjacent neurons. *J Neurophysiol* **91**, 2782-2796, doi:10.1152/jn.01267.2003 (2004).
- 649 43 Hasenstaub, A. *et al.* Inhibitory postsynaptic potentials carry synchronized frequency
650 information in active cortical networks. *Neuron* **47**, 423-435,
651 doi:10.1016/j.neuron.2005.06.016 (2005).
- 652 44 Kass, R. E., Ventura, V. & Cai, C. Statistical smoothing of neuronal data. *Network* **14**, 5-
653 15, doi:10.1088/0954-898x/14/1/301 (2003).
- 654 45 Shimazaki, H. & Shinomoto, S. Kernel bandwidth optimization in spike rate estimation. *J*
655 *Comput Neurosci* **29**, 171-182, doi:10.1007/s10827-009-0180-4 (2010).
- 656 46 Westheimer, G. Mechanism of saccadic eye movements. *AMA Arch Ophthalmol* **52**, 710-
657 724, doi:10.1001/archophth.1954.00920050716006 (1954).
- 658 47 Pare, M. & Munoz, D. P. Saccadic reaction time in the monkey: Advanced preparation of
659 oculomotor programs is primarily responsible for express saccade occurrence. *Journal of*
660 *Neurophysiology* **76**, 3666-3681 (1996).
- 661 48 Deubel, H. & Schneider, W. X. Saccade target selection and object recognition: evidence
662 for a common attentional mechanism. *Vision Res* **36**, 1827-1837, doi:10.1016/0042-
663 6989(95)00294-4 (1996).
- 664 49 Gilzenrat, M. S., Nieuwenhuis, S., Jepma, M. & Cohen, J. D. Pupil diameter tracks changes
665 in control state predicted by the adaptive gain theory of locus coeruleus function. *Cogn*
666 *Affect Behav Neurosci* **10**, 252-269, doi:10.3758/CABN.10.2.252 (2010).
- 667 50 Reimer, J. *et al.* Pupil fluctuations track fast switching of cortical states during quiet
668 wakefulness. *Neuron* **84**, 355-362, doi:10.1016/j.neuron.2014.09.033 (2014).
- 669 51 Jainta, S., Vernet, M., Yang, Q. & Kapoula, Z. The pupil reflects motor preparation for
670 saccades-even before the eye starts to move. *Frontiers in human neuroscience* **5**, 97 (2011).
- 671 52 Doiron, B., Litwin-Kumar, A., Rosenbaum, R., Ocker, G. K. & Josic, K. The mechanics
672 of state-dependent neural correlations. *Nat Neurosci* **19**, 383-393, doi:10.1038/nn.4242
673 (2016).
- 674 53 Mitchell, J. F., Sundberg, K. A. & Reynolds, J. H. Spatial attention decorrelates intrinsic
675 activity fluctuations in macaque area V4. *Neuron* **63**, 879-888,
676 doi:10.1016/j.neuron.2009.09.013 (2009).

- 677 54 Cohen, M. R. & Maunsell, J. H. Attention improves performance primarily by reducing
678 interneuronal correlations. *Nat Neurosci* **12**, 1594-1600, doi:10.1038/nn.2439 (2009).
- 679 55 Anastassiou, C. A., Perin, R., Markram, H. & Koch, C. Ephaptic coupling of cortical
680 neurons. *Nat Neurosci* **14**, 217-223, doi:10.1038/nn.2727 (2011).
- 681 56 Fries, P. Rhythms for Cognition: Communication through Coherence. *Neuron* **88**, 220-235,
682 doi:10.1016/j.neuron.2015.09.034 (2015).
- 683 57 Sirota, A. *et al.* Entrainment of neocortical neurons and gamma oscillations by the
684 hippocampal theta rhythm. *Neuron* **60**, 683-697, doi:10.1016/j.neuron.2008.09.014 (2008).
- 685 58 Veit, J., Hakim, R., Jadi, M. P., Sejnowski, T. J. & Adesnik, H. Cortical gamma band
686 synchronization through somatostatin interneurons. *Nature neuroscience* **20**, 951 (2017).
- 687 59 Ozeki, H., Finn, I. M., Schaffer, E. S., Miller, K. D. & Ferster, D. Inhibitory stabilization
688 of the cortical network underlies visual surround suppression. *Neuron* **62**, 578-592,
689 doi:10.1016/j.neuron.2009.03.028 (2009).
- 690 60 Tsodyks, M. V., Skaggs, W. E., Sejnowski, T. J. & McNaughton, B. L. Paradoxical effects
691 of external modulation of inhibitory interneurons. *J Neurosci* **17**, 4382-4388 (1997).
- 692 61 Douglas, R. J. & Martin, K. A. Mapping the matrix: the ways of neocortex. *Neuron* **56**,
693 226-238, doi:10.1016/j.neuron.2007.10.017 (2007).
- 694 62 Bair, W., Zohary, E. & Newsome, W. T. Correlated firing in macaque visual area MT: time
695 scales and relationship to behavior. *J Neurosci* **21**, 1676-1697 (2001).
- 696 63 Kohn, A. & Smith, M. A. Stimulus dependence of neuronal correlation in primary visual
697 cortex of the macaque. *J Neurosci* **25**, 3661-3673, doi:10.1523/JNEUROSCI.5106-
698 04.2005 (2005).
- 699 64 Shadlen, M. N. & Newsome, W. T. The variable discharge of cortical neurons: implications
700 for connectivity, computation, and information coding. *J Neurosci* **18**, 3870-3896 (1998).
- 701 65 Kriener, B., Tetzlaff, T., Aertsen, A., Diesmann, M. & Rotter, S. Correlations and
702 population dynamics in cortical networks. *Neural Comput* **20**, 2185-2226,
703 doi:10.1162/neco.2008.02-07-474 (2008).
- 704 66 Saalmann, Y. B., Pinsk, M. A., Wang, L., Li, X. & Kastner, S. The pulvinar regulates
705 information transmission between cortical areas based on attention demands. *Science* **337**,
706 753-756, doi:10.1126/science.1223082 (2012).
- 707 67 Zhou, H., Schafer, R. J. & Desimone, R. Pulvinar-Cortex Interactions in Vision and
708 Attention. *Neuron* **89**, 209-220, doi:10.1016/j.neuron.2015.11.034 (2016).

- 709 68 Petersen, S. E., Robinson, D. L. & Morris, J. D. Contributions of the pulvinar to visual
710 spatial attention. *Neuropsychologia* **25**, 97-105, doi:10.1016/0028-3932(87)90046-7
711 (1987).
- 712 69 Wilke, M., Turchi, J., Smith, K., Mishkin, M. & Leopold, D. A. Pulvinar inactivation
713 disrupts selection of movement plans. *J Neurosci* **30**, 8650-8659,
714 doi:10.1523/JNEUROSCI.0953-10.2010 (2010).
- 715 70 Wilke, M., Kagan, I. & Andersen, R. A. Effects of pulvinar inactivation on spatial decision-
716 making between equal and asymmetric reward options. *J Cogn Neurosci* **25**, 1270-1283,
717 doi:10.1162/jocn_a_00399 (2013).
- 718 71 Kawaguchi, Y. & Kubota, Y. Correlation of physiological subgroupings of nonpyramidal
719 cells with parvalbumin- and calbindinD28k-immunoreactive neurons in layer V of rat
720 frontal cortex. *J Neurophysiol* **70**, 387-396, doi:10.1152/jn.1993.70.1.387 (1993).
- 721 72 Galarreta, M. & Hestrin, S. A network of fast-spiking cells in the neocortex connected by
722 electrical synapses. *Nature* **402**, 72-75, doi:10.1038/47029 (1999).
- 723 73 Cruikshank, S. J., Urabe, H., Nurmikko, A. V. & Connors, B. W. Pathway-specific
724 feedforward circuits between thalamus and neocortex revealed by selective optical
725 stimulation of axons. *Neuron* **65**, 230-245, doi:10.1016/j.neuron.2009.12.025 (2010).
- 726 74 Gibson, J. R., Beierlein, M. & Connors, B. W. Two networks of electrically coupled
727 inhibitory neurons in neocortex. *Nature* **402**, 75-79, doi:10.1038/47035 (1999).
- 728 75 Agmon, A. & Connors, B. W. Correlation between Intrinsic Firing Patterns and
729 Thalamocortical Synaptic Responses of Neurons in Mouse Barrel Cortex. *Journal of*
730 *Neuroscience* **12**, 319-329 (1992).
- 731 76 Poulet, J. F. & Petersen, C. C. Internal brain state regulates membrane potential synchrony
732 in barrel cortex of behaving mice. *Nature* **454**, 881-885, doi:10.1038/nature07150 (2008).
- 733 77 Vinck, M., Batista-Brito, R., Knoblich, U. & Cardin, J. A. Arousal and locomotion make
734 distinct contributions to cortical activity patterns and visual encoding. *Neuron* **86**, 740-754,
735 doi:10.1016/j.neuron.2015.03.028 (2015).
- 736 78 Arroyo, S., Bennett, C. & Hestrin, S. Correlation of Synaptic Inputs in the Visual Cortex
737 of Awake, Behaving Mice. *Neuron* **99**, 1289-1301 e1282,
738 doi:10.1016/j.neuron.2018.08.008 (2018).
- 739 79 John, E. R. *et al.* Invariant reversible QEEG effects of anesthetics. *Conscious Cogn* **10**,
740 165-183, doi:10.1006/ccog.2001.0507 (2001).
- 741 80 Zohary, E., Shadlen, M. N. & Newsome, W. T. Correlated neuronal discharge rate and its
742 implications for psychophysical performance. *Nature* **370**, 140-143,
743 doi:10.1038/370140a0 (1994).

- 744 81 Abbott, L. F. & Dayan, P. The effect of correlated variability on the accuracy of a
745 population code. *Neural Comput* **11**, 91-101, doi:10.1162/089976699300016827 (1999).
- 746 82 Bartolo, R., Saunders, R. C., Mitz, A. R. & Averbeck, B. B. Information-Limiting
747 Correlations in Large Neural Populations. *J Neurosci* **40**, 1668-1678,
748 doi:10.1523/JNEUROSCI.2072-19.2019 (2020).
- 749 83 Averbeck, B. B., Latham, P. E. & Pouget, A. Neural correlations, population coding and
750 computation. *Nat Rev Neurosci* **7**, 358-366, doi:10.1038/nrn1888 (2006).
- 751 84 Nassi, J. J., Avery, M. C., Cetin, A. H., Roe, A. W. & Reynolds, J. H. Optogenetic
752 Activation of Normalization in Alert Macaque Visual Cortex. *Neuron* **86**, 1504-1517,
753 doi:10.1016/j.neuron.2015.05.040 (2015).
- 754 85 Ruiz, O. *et al.* Optogenetics through windows on the brain in the nonhuman primate. *J*
755 *Neurophysiol* **110**, 1455-1467, doi:10.1152/jn.00153.2013 (2013).
- 756 86 Konig, S. D. & Buffalo, E. A. A nonparametric method for detecting fixations and saccades
757 using cluster analysis: removing the need for arbitrary thresholds. *J Neurosci Methods* **227**,
758 121-131, doi:10.1016/j.jneumeth.2014.01.032 (2014).
- 759 87 Mitra, P. P. & Pesaran, B. Analysis of dynamic brain imaging data. *Biophys J* **76**, 691-708,
760 doi:10.1016/S0006-3495(99)77236-X (1999).
- 761 88 Zeitler, M., Fries, P. & Gielen, S. Assessing neuronal coherence with single-unit, multi-
762 unit, and local field potentials. *Neural Comput* **18**, 2256-2281,
763 doi:10.1162/neco.2006.18.9.2256 (2006).
- 764 89 Vinck, M., Battaglia, F. P., Womelsdorf, T. & Pennartz, C. Improved measures of phase-
765 coupling between spikes and the Local Field Potential. *J Comput Neurosci* **33**, 53-75,
766 doi:10.1007/s10827-011-0374-4 (2012).
767

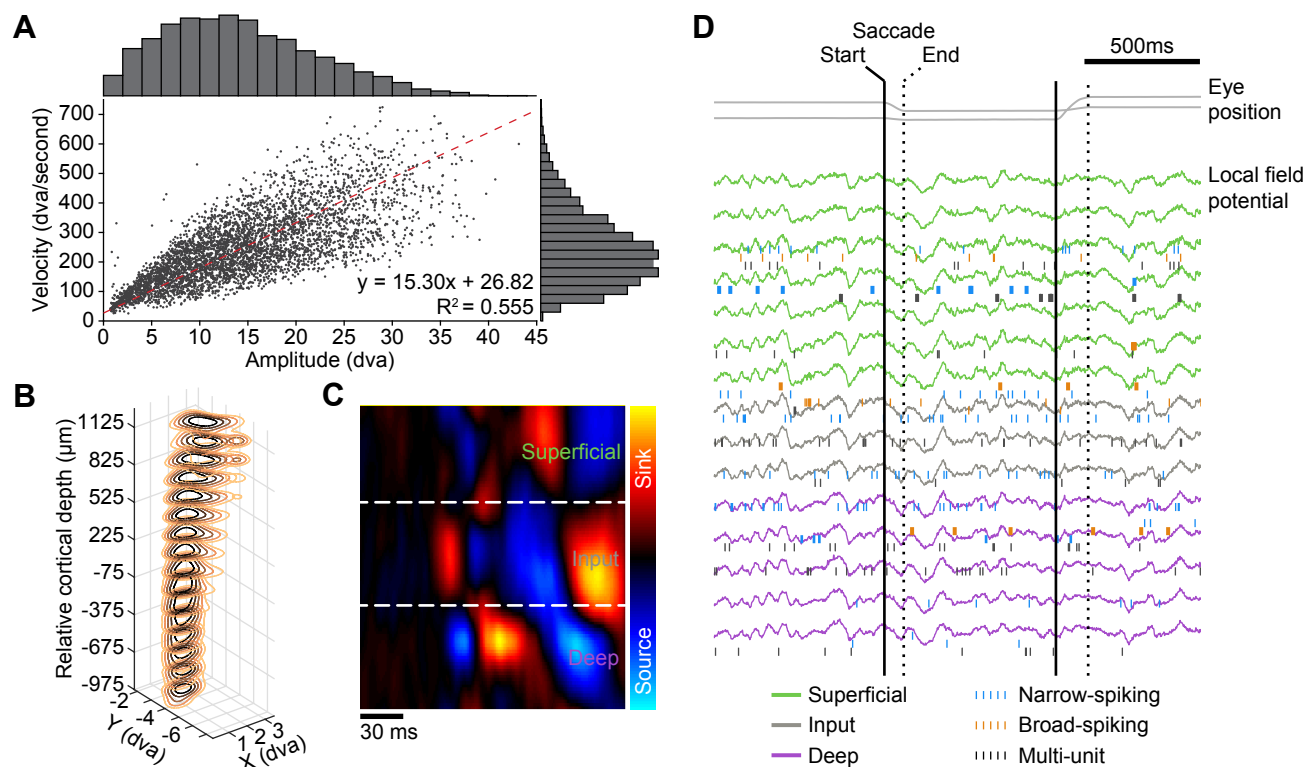


Figure 1. Laminar Recordings and Saccade Identification

(A) The amplitude-velocity relationship ('main sequence') for all saccades ($n = 4420$) in the dataset. An approximately linear trend is expected for saccades, as is found here ($R^2 = 0.555$). dva = degrees of visual angle.

(B) Stacked contour plot showing spatial receptive fields (RFs) along the laminar probe from an example session. The RFs are well aligned, indicating perpendicular penetration down a cortical column. Zero depth represents the center of the input layer as estimated with current source density (CSD) analysis.

(C) CSD displayed as a colored map. The x-axis represents time from stimulus onset; the y-axis represents cortical depth. The CSD map has been spatially smoothed for visualization.

(D) Example of continuous eye-tracker and electrophysiological recordings. Eye traces are plotted at the top in grey. LFP traces are plotted by depth below, and spikes are overlaid on the corresponding channel. LFP traces have been color coded by layer identity; spikes have been color coded by cell type.

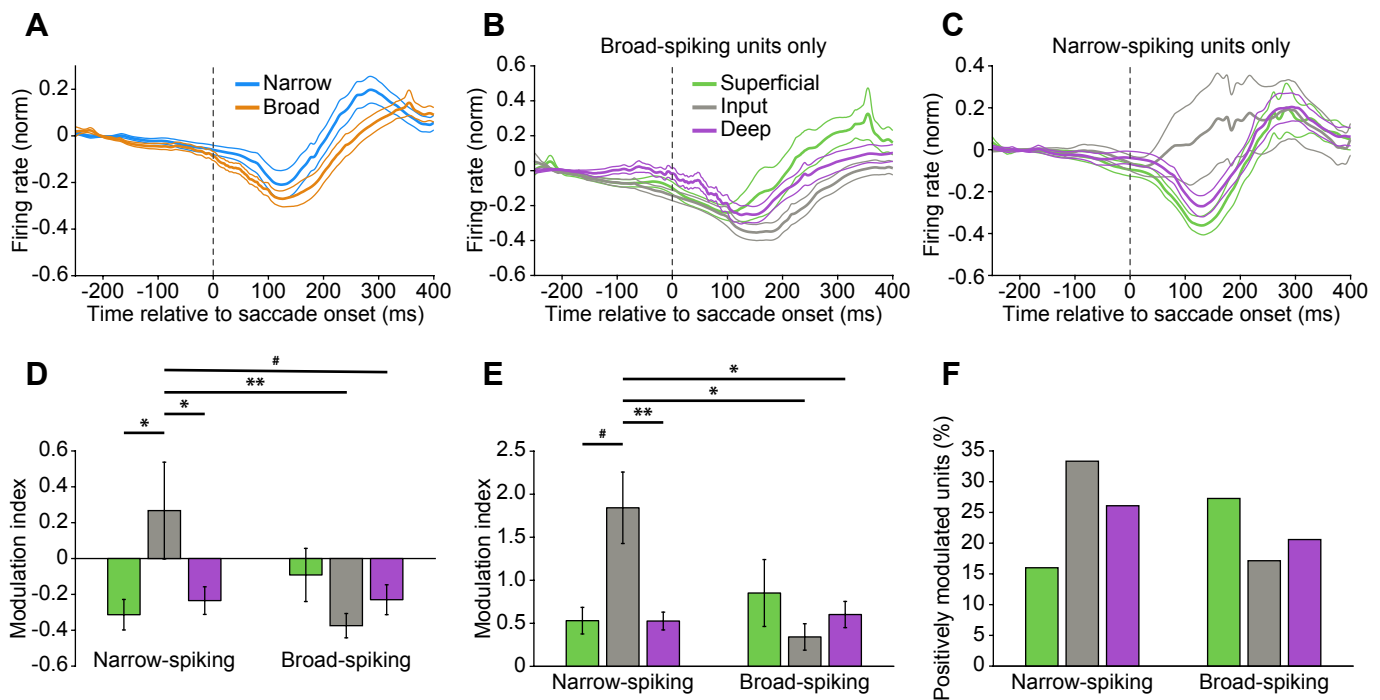


Figure 2. Narrow-Spiking Input Layer Units Display Peri-Saccadic Enhancement of Firing

(A) Average peri-saccadic normalized firing rate for broad- ($n = 102$ units) and narrow-spiking ($n = 95$ units) populations. Thin lines indicate standard error of the mean.

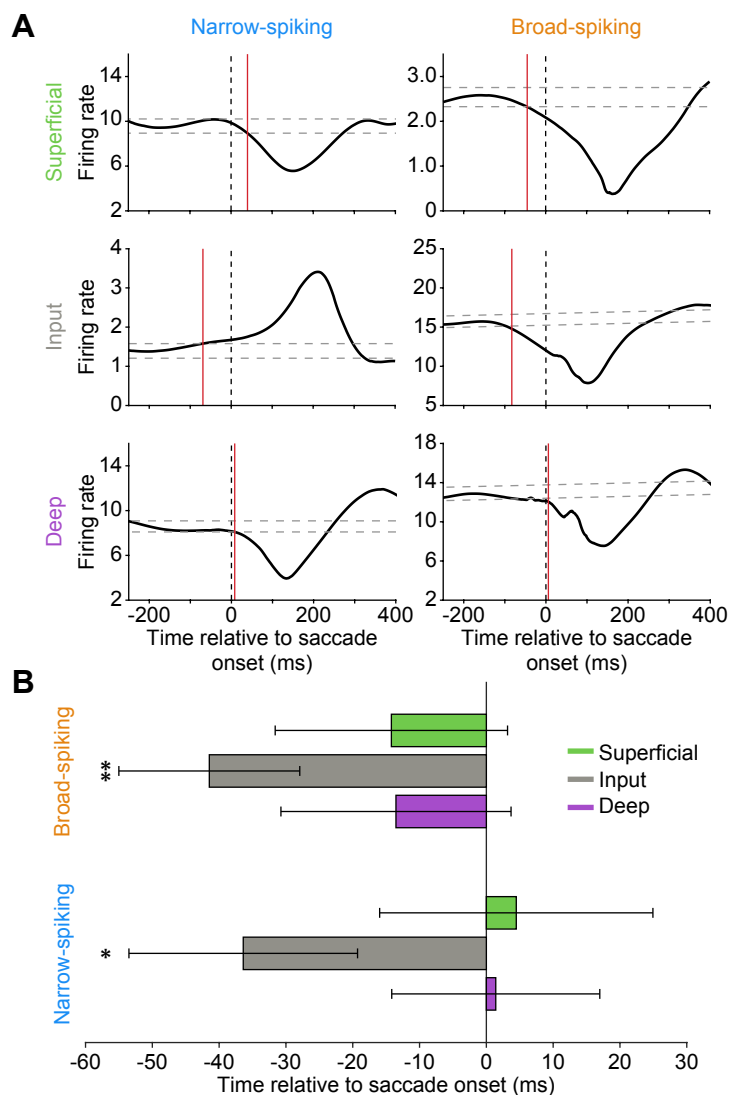
(B) As in (A), but including only broad-spiking units from the superficial ($n = 33$), input ($n = 35$), and deep ($n = 34$) layer populations.

(C) As in (A), but including only narrow-spiking units from the superficial ($n = 25$ units), input ($n = 24$ units), and deep ($n = 46$ units) layer populations.

(D) Average peri-saccadic modulation index for the six neural subpopulations. Two-way ANOVA ($F_{layer} = 1.16$, $P = 0.3151$; $F_{cell\ type} = 1.84$, $P = 0.1765$; $F_{interaction} = 5.98$, $P = 0.0030$) with Tukey's multiple comparison tests (narrow-spiking superficial vs narrow-spiking input, $*P = 0.0423$; narrow-spiking input vs narrow-spiking deep, $*P = 0.0495$; narrow-spiking input vs broad-spiking input, $**P = 0.0070$; narrow-spiking input vs broad-spiking deep, $\#P = 0.0817$). Error bars indicate standard error of the mean.

(E) Average peri-saccadic modulation index for positively modulated units from the six neural subpopulations. Two-way ANOVA ($F_{layer} = 1.87$, $P = 0.1666$; $F_{cell\ type} = 2.32$, $P = 0.1355$; $F_{interaction} = 5.51$, $P = 0.0077$) with Tukey's multiple comparison tests (narrow-spiking superficial vs narrow-spiking input, $\#P = 0.0833$; narrow-spiking input vs narrow-spiking deep, $**P = 0.0073$; narrow-spiking input vs broad-spiking input, $*P = 0.0106$; narrow-spiking input vs broad-spiking deep, $*P = 0.0384$). Error bars indicate standard error of the mean.

(F) Proportion of units in each neural subpopulation with a positive peri-saccadic modulation index.



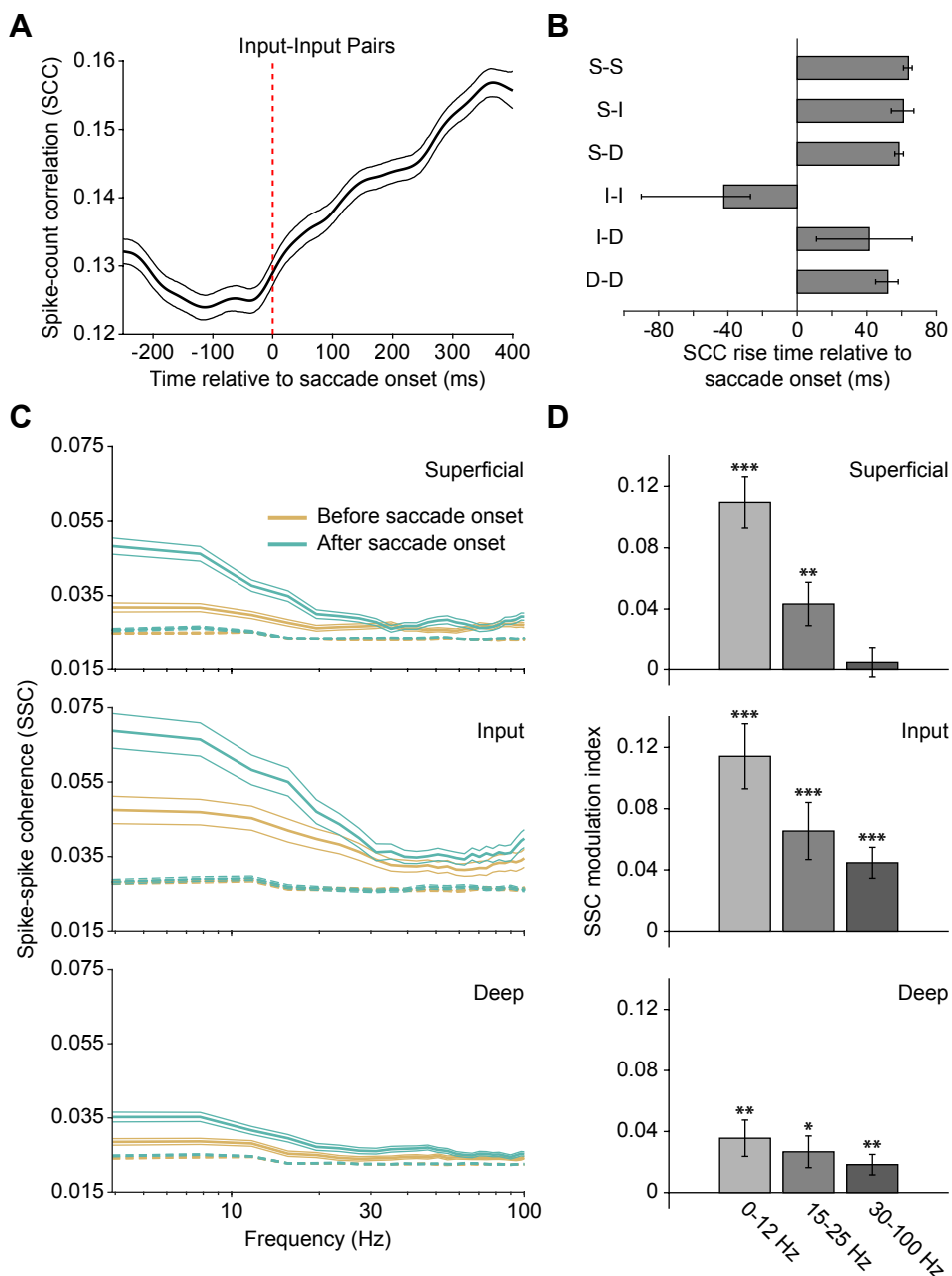


Figure 4. Saccade Onset Increases Correlated Variability Most Prominently in the Input Layer

(A) Spike count correlations as a function of time relative to saccade onset for input-input unit pairs ($n = 240$ pairs). Correlations were calculated with a sliding 201 ms window. Thin lines indicate bootstrapped 95% confidence intervals.

(B) Average start time of spike count correlation rise relative to saccade onset. Y-axis labels indicate layer identity of unit pairs (S - superficial; I - input; D - deep). Error bars represent bootstrapped 95% confidence intervals. Input-input pairs begin to rise before saccade onset and before all other pair combinations. All other pairs respond after saccade onset.

(C) Average spike-spike coherence between pairs of simultaneously recorded units (single-units and multi-units) before (-200 to 0 ms) and after (0 to 200 ms) saccade onset as a function of frequency. Superficial layer, $n = 299$ pairs; input layer, $n = 191$ pairs; deep layer, $n = 604$ pairs. Thin lines indicate standard error of the mean. Dashed lines indicate spike-spike coherence for shuffled data.

(D) Same data as in (C), but averaged across three frequency bands and plotted as a modulation index: $(SSC_{after} - SSC_{before}) / (SSC_{after} + SSC_{before})$. Two-tailed one-sample t-tests (Superficial 0-12 Hz, $***P = 1.64 \times 10^{-10}$; Superficial 15-25 Hz, $**P = 0.0027$; Superficial 30-100 Hz, $P = 0.5468$; Input 0-12 Hz, $***P = 2.2131 \times 10^{-7}$; Input 15-25 Hz, $***P = 5.5458 \times 10^{-4}$; Input 30-100 Hz, $***P = 1.6503 \times 10^{-5}$; Deep 0-12 Hz, $**P = 0.0013$; Deep 15-25 Hz, $*P = 0.0116$; Deep 30-100 Hz, $**P = 0.0050$). Error bars indicate standard error of the mean.

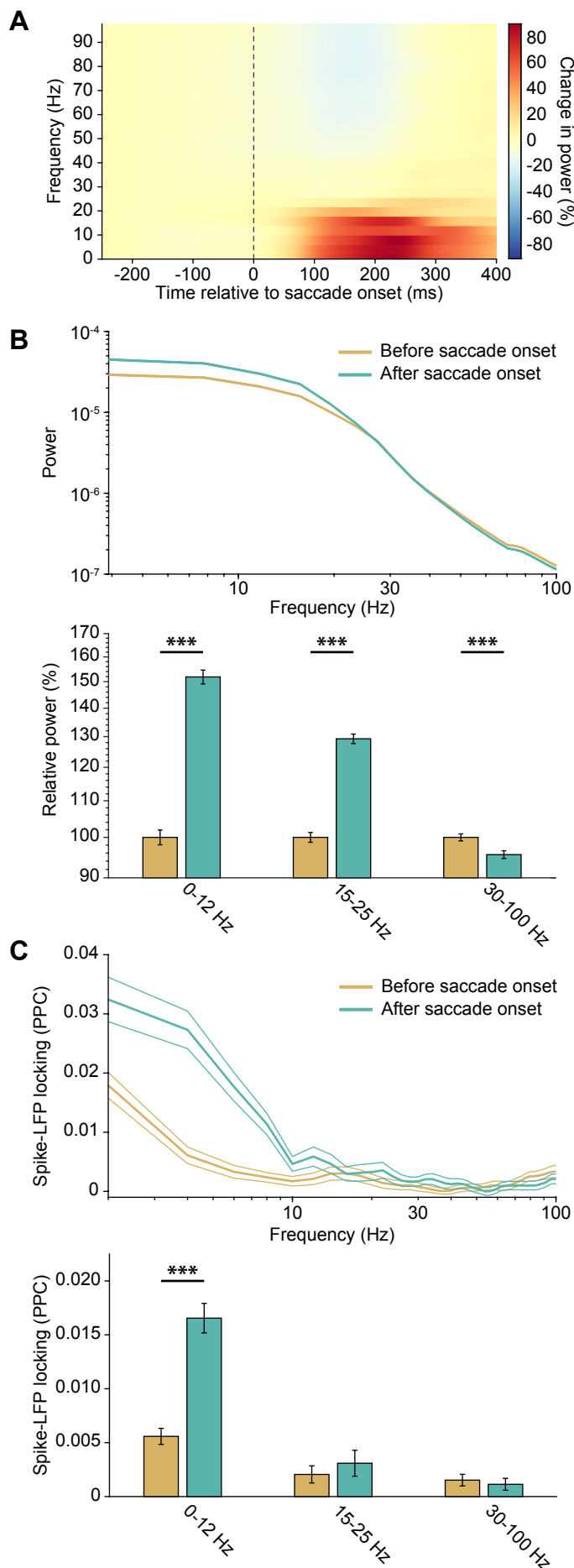


Figure 5. Saccade Onset Increases Low Frequency Power and Spike-LFP Locking

(A) Time-frequency representation (spectrogram) of LFP power around saccade onset. Signal strength is represented as percent change in power (i.e. the raw power at each timepoint is divided by the average power in the baseline period, defined here as 250 to 150 ms before saccade onset).

(B) Top: Average power spectra before (-200 to 0 ms) and after (0 to 200 ms) saccade onset. Thin lines indicate standard error of the mean. Bottom: Same data as in top, but averaged across three frequency bands and normalized to data before saccade onset for visualization. Two tailed paired-sample t-tests (0-12 Hz, $***P = 3.4669 \times 10^{-92}$; 15-25 Hz, $***P = 9.3690 \times 10^{-74}$; 30-100 Hz, $***P = 2.7322 \times 10^{-9}$). Error bars indicate standard error of the mean.

(C) Top: Average spike-LFP locking spectra before (-200 to 0 ms) and after (0 to 200 ms) saccade onset. Thin lines indicate standard error of the mean. Bottom: Same data as in top, but averaged across three frequency bands. Two tailed paired-sample t-tests (0-12 Hz, $***P = 1.7147 \times 10^{-19}$; 15-25 Hz, $P = 0.1598$; 30-100 Hz, $P = 0.1091$). Error bars indicate standard error of the mean.

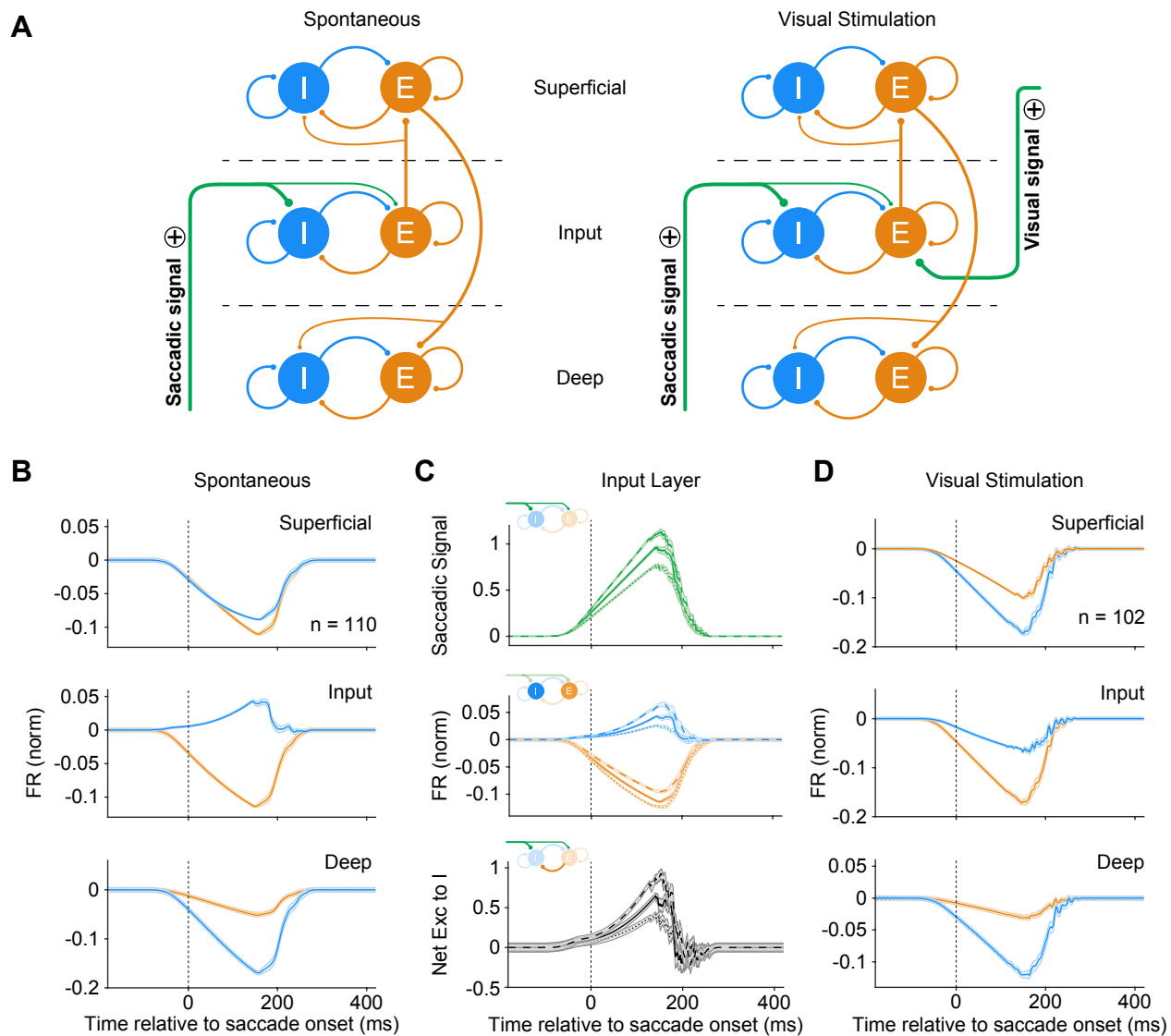


Figure 6. A Computational Model Confirms that Activation of an Input Layer-Targeting Projection Induces Saccadic Suppression

(A) Connectivity between populations in our computational model. Excitatory (E) and inhibitory (I) populations within each layer project to each other as well as themselves. The input layer excitatory population projects to the superficial layer, while the superficial excitatory population projects to the deep layer. In our model of spontaneous saccades (left), we activate an external excitatory projection that selectively targets the input layer. In our model of saccades executed in the presence of visual stimuli (right), we add an additional input that selectively targets input layer excitatory neurons.

(B) Normalized peri-saccadic firing rate of simulated neural subpopulations during spontaneously executed saccades ($n = 110$ simulated saccades). The input layer inhibitory subpopulation shows enhancement of firing, while all other subpopulations show suppression.

(C) Further dissection of input layer activity. (Top) The saccadic signal arriving in the input layer was simulated with a ramping function. Represented here are saccadic signals of three different strengths. From weakest to strongest, these are represented by dotted, continuous, and dashed lines, both here and in the following subpanels. (Middle) The excitatory and inhibitory input layer subpopulation firing rates in response to three saccadic signals of varying strength. (Bottom) Net excitatory drive onto the inhibitory input layer subpopulation in response to three saccadic signals of varying strength. The excitatory drive is the sum of drive from the external saccadic input and drive from the local excitatory population.

(D) Normalized peri-saccadic firing rate of simulated neural subpopulations during saccades executed in the presence of visual stimulation ($n = 102$ simulated saccades). Visual stimulation is represented by the activation of a second input, which selectively targets the input layer excitatory subpopulation. Here, all subpopulations within the cortical column show peri-saccadic suppression.

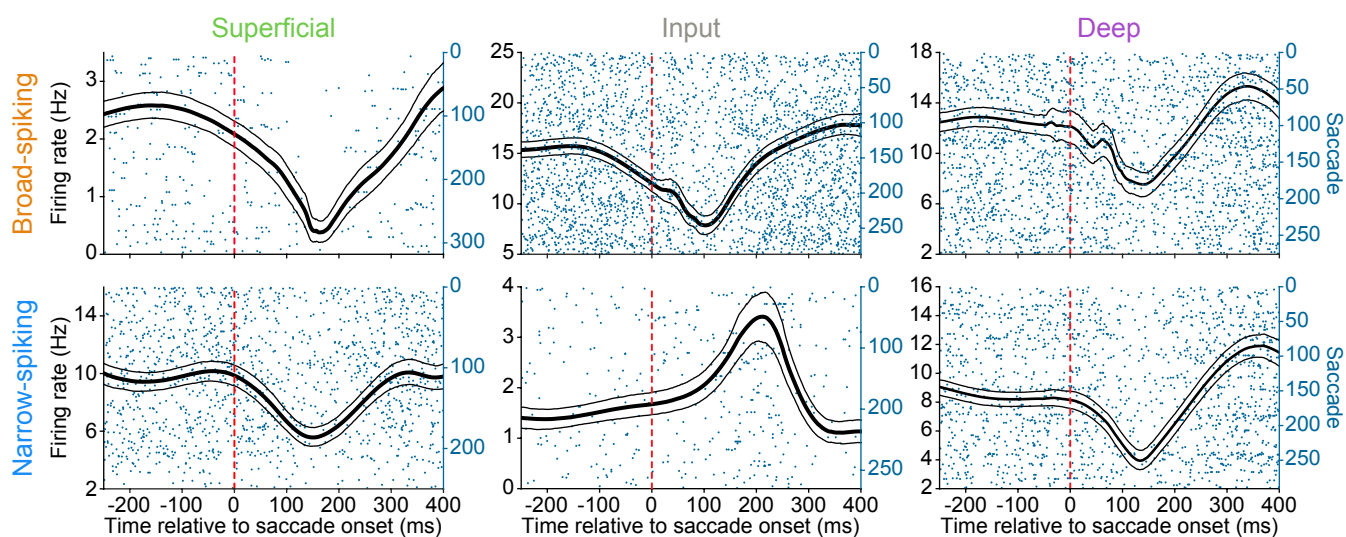


Figure S1. Peri-Saccadic Single-Unit Firing Rate Estimation

Peri-saccadic single-unit firing rates were estimated by smoothing individual spikes with gaussian kernels. The kernel bandwidth was selected for each unit at each point in time using an optimization algorithm that minimizes the mean integrated squared error⁴⁵. The firing rate estimates produced by this approach are shown for six representative example units, one from each recorded neural subpopulation. The smoothed firing rates (black) are overlaid on the raster plots showing raw spikes (blue). In the raster plot, each row represents a single saccade. Thin lines are bootstrapped 95% confidence intervals of the firing rate estimate.

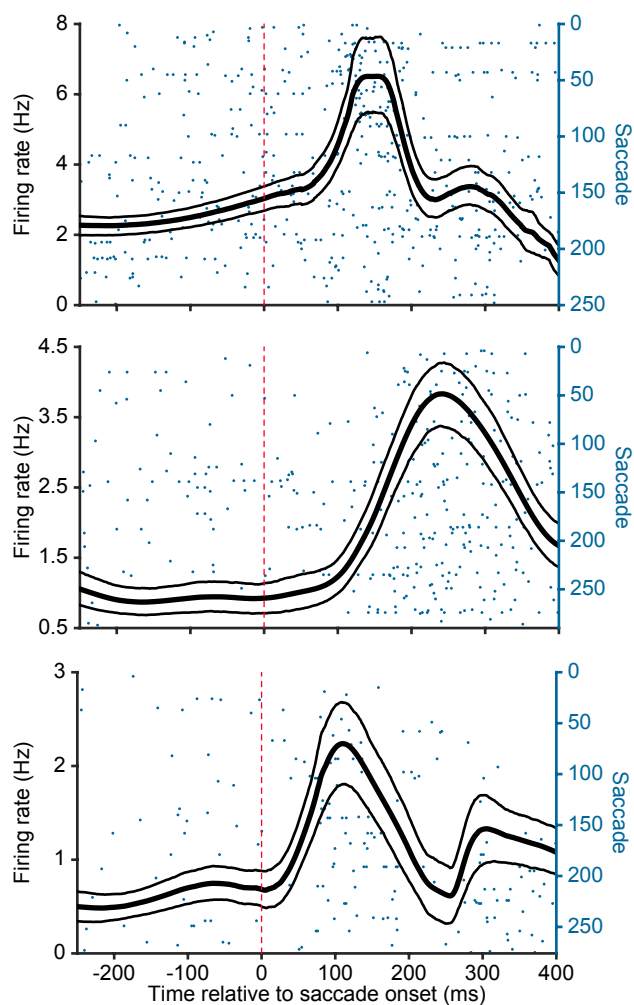


Figure S2. Additional Narrow-Spiking Input Layer Single-Unit Examples

Additional example narrow-spiking input layer single-units that display peri-saccadic enhancement of firing. Firing rates were estimated using a kernel smoothing approach and bandwidth optimization algorithm⁴⁵. The smoothed firing rates (black) are overlaid on the spike raster plots (blue). Thin lines are bootstrapped 95% confidence intervals of the firing rate estimate.

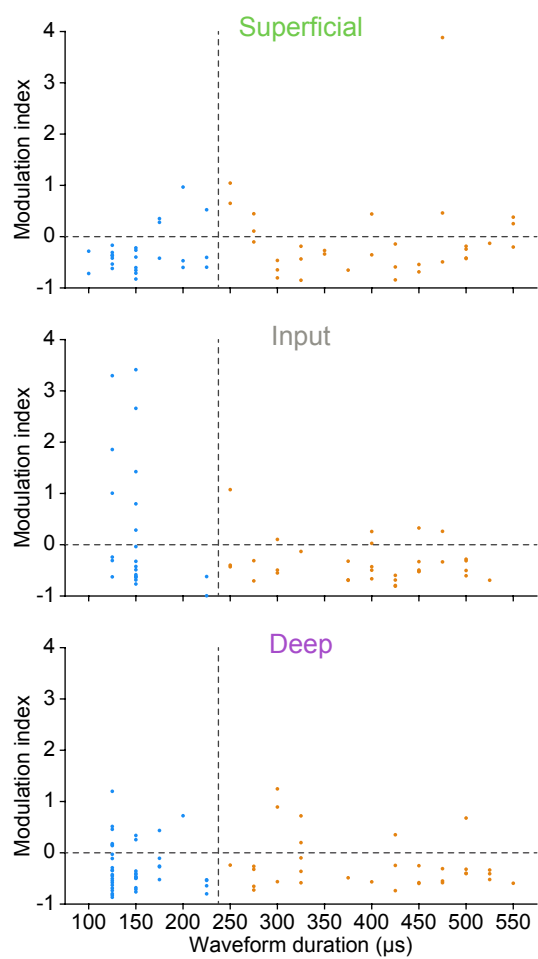


Figure S3. Single-Unit Modulation Indices

Single-unit modulation indices as a function of spike waveform duration. Neural populations from each layer are displayed in different subplots. The dashed horizontal line represents a modulation index of zero (no firing rate change), while the dashed vertical line represents the threshold separating narrow- and broad- spiking units.

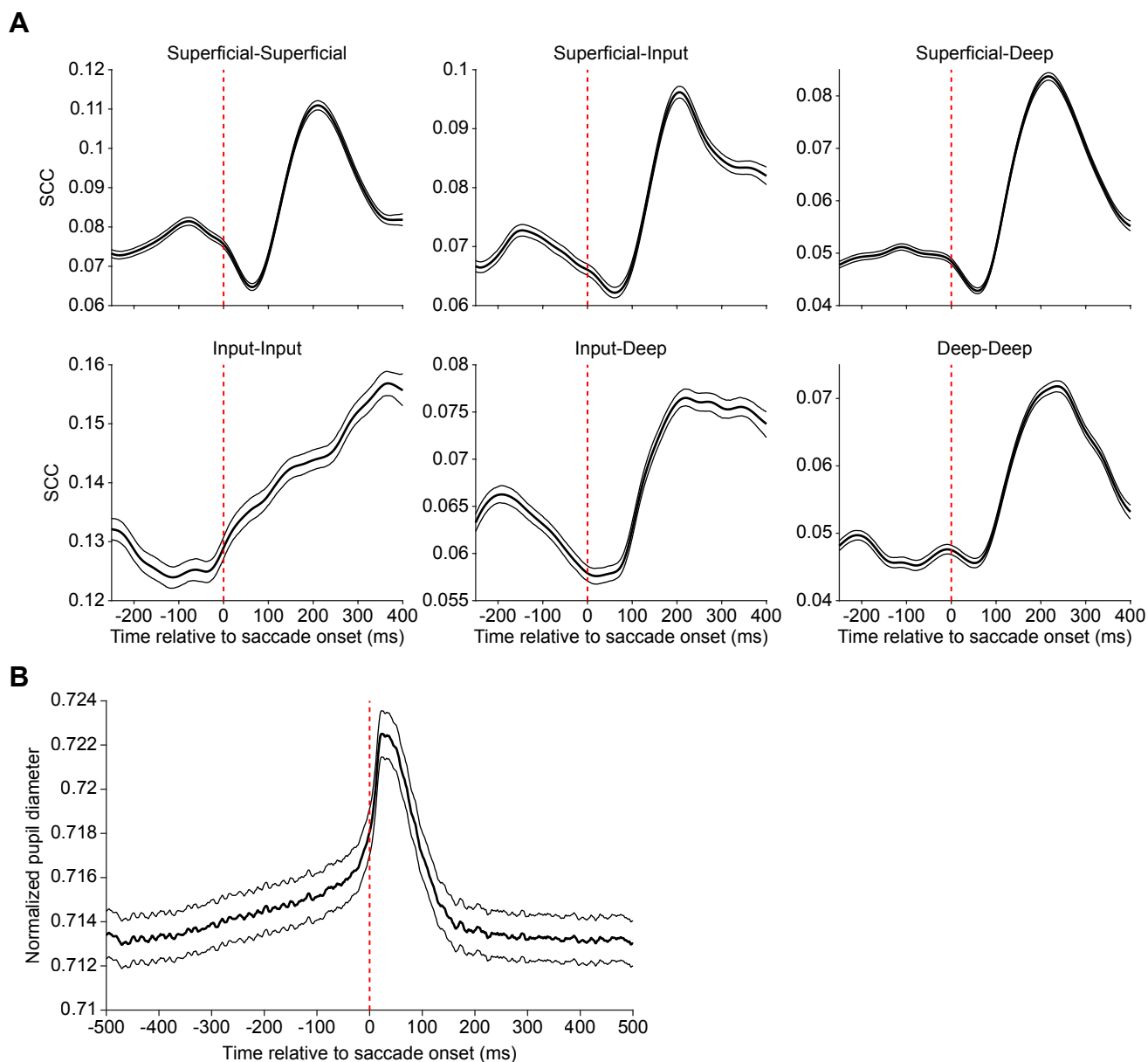


Figure S4. Input Layer Pairs Show Increases in Spike Count Correlations Prior to Saccade Onset

(A) Spike count correlations as a function of time relative to saccade onset for all combinations of layer-wise unit pairs. Superficial-superficial, $n = 442$ pairs; superficial-input, $n = 558$ pairs; superficial-deep, $n = 755$ pairs; input-input, $n = 240$ pairs; input-deep, $n = 501$ pairs; deep-deep, $n = 680$ pairs. Correlations were calculated with a sliding 201 ms window. Thin lines indicate bootstrapped 95% confidence intervals.

(B) Normalized pupil diameter around the time of saccade onset ($n = 4420$ saccades). Thin lines indicate standard error of the mean.

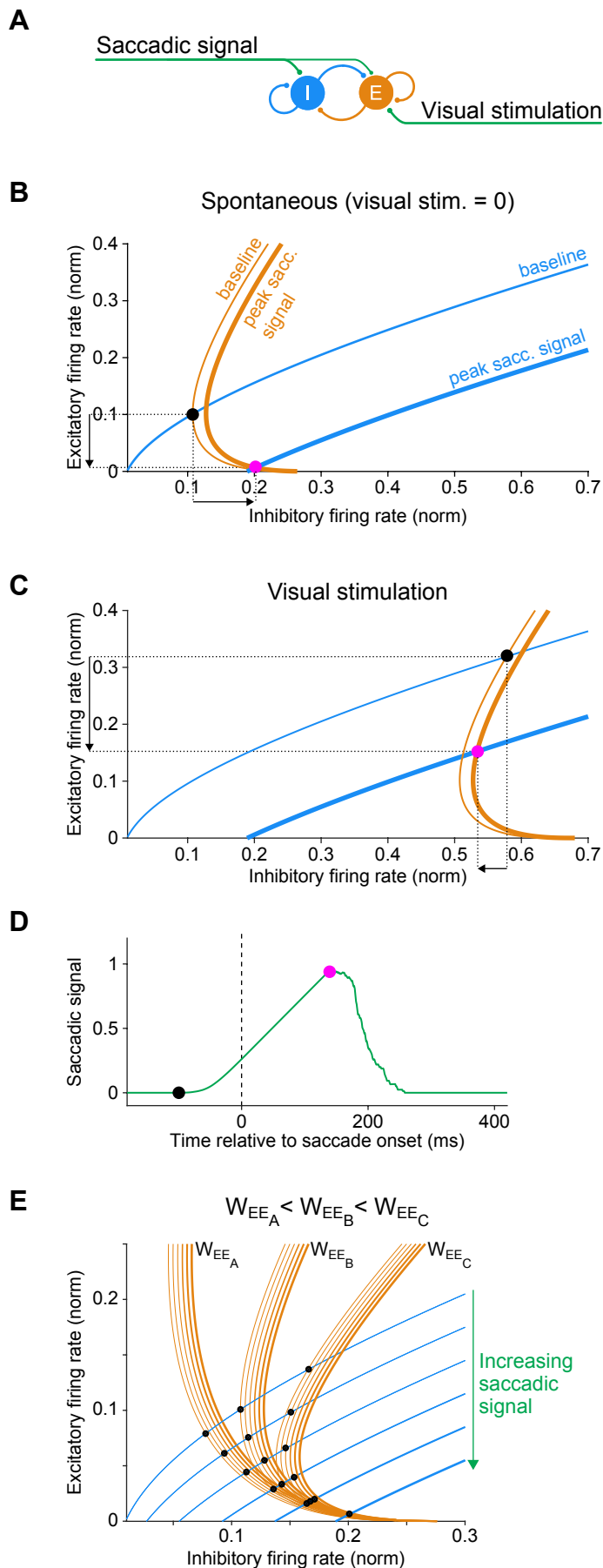


Figure S5. Phase Plane Analysis of the Input Layer E-I System

(A) The E-I network in the input layer.

(B) The nullclines and stable activity levels of the input layer E and I populations during simulation of spontaneous activity. Equations and parameters are the same as those described in the Methods and used in Figure 6. The orange and blue curves show the E and I nullclines, respectively, of the E-I network in (A). Each point on a nullcline indicates the steady state firing rate of the E or I population when the activity of the other population is fixed, i.e. the rate of change in equations (3) or (4) is zero. The ISN and non-ISN regimes of the network are demarcated by the switch between positive and negative slopes along the E nullclines. This ability to switch is a consequence of strong E-E connectivity, and is absent when the E-E connectivity strength is either weak or zero. The thin nullclines depict firing rates when saccadic input is at baseline; the thick nullclines depict firing rates when saccadic input increases by a non-zero value. The intersections of the E and I nullclines indicate the steady state firing rates at which the network stabilizes if allowed to seek equilibrium (indicated by black and pink dots at baseline and during peak saccadic suppression, respectively). As illustrated here, the nullclines for our model intersect in the non-ISN regime in the absence of visual input, causing E and I activity to shift in opposite directions in response to the saccadic signal.

(C) Same as in (B), but during simulated visual stimulation. The addition of excitatory input to the E population shifts the E nullclines to the right, causing them to intersect with the I nullclines in the ISN regime. As illustrated here, this causes the E and I populations to shift in the same direction in response to the saccadic signal.

(D) The approximate level of saccadic signal strength that corresponds to the E (orange) and I (blue) nullcline sets shown in (B) and (C). The phase plane analysis is most applicable to constant levels of saccadic signal, and is only an approximate depiction of the scenario of a ramp signal shown in (D), and as used in the model simulation in Figure 6.

(E) Effect of E-E connection strength on inhibitory firing rate changes in response to the saccadic signal. Each set of E nullclines corresponds to a given E-E connection strength (W_{EE}), and illustrates the effects of raising saccadic signal magnitude (indicated by greater line thickness), causing either increases or decreases in steady state firing rates (black dots), as determined by their intersection with the I nullclines. This phase plane analysis approximately predicts three ways in which I firing rate can shift in response to increasing saccadic input: 1) it increases quickly in response to a small increase in saccadic signal (W_{EE_A}), 2) it increases minimally until a threshold level of saccadic signal is reached (W_{EE_B}), or 3) it first decreases then increases with rising saccadic signal strength (W_{EE_C}). The operating regime shown in the simulation results (Figure 6) that recapitulate experimental observations corresponds to the E-E connection strength illustrated by W_{EE_B} . In this case, the network is maintained at the boundary between ISN (positive E nullcline slope) and non-ISN (negative E nullcline slope) regimes in the absence of the saccadic signal.